nature plants

Article

https://doi.org/10.1038/s41477-023-01390-4

FERONIA coordinates plant growth and salt tolerance via the phosphorylation of phyB

Received: 19 March 2022

Accepted: 9 March 2023

Published online: 03 April 2023

Check for updates

Xin Liu[1,2], Wei Jiang[1], Yali Li[1,2], Haozhen Nie[3], Lina Cui[2,4], Rongxia Li[5], Li Tan[1], Li Peng[1], Chao Li[1], Jinyan Luo[1], Ming Li[1], Hongxia Wang[3], Jun Yang[3], Bing Zhou[2,4,6,7], Pengcheng Wang[1], Hongtao Liu[8], Jian-Kang Zhu[1,9,10,11] & Chunzhao Zhao[1]

Phosphorylation modification is required for the modulation of phytochrome B (phyB) thermal reversion, but the kinase(s) that phosphorylate(s) phyB and the biological significance of the phosphorylation are still unknown. Here we report that FERONIA (FER) phosphorylates phyB to regulate plant growth and salt tolerance, and the phosphorylation not only regulates dark-triggered photobody dissociation but also modulates phyB protein abundance in the nucleus. Further analysis indicates that phosphorylation of phyB by FER is sufficient to accelerate the conversion of phyB from the active form (Pfr) to the inactive form (Pr). Under salt stress, FER kinase activity is inhibited, leading to delayed photobody dissociation and increased phyB protein abundance in the nucleus. Our data also show that *phyB* mutation or overexpression of *PIF5* attenuates growth inhibition and promotes plant survival under salt stress. Together, our study not only reveals a kinase that controls phyB turnover via a signature of phosphorylation, but also provides mechanistic insights into the role of the FER-phyB module in coordinating plant growth and stress tolerance.

Phytochromes are photoreceptors that are essential for the sensing and transduction of red (R) and far-red (FR) light signals, thus facilitating the response of plants to ever-changing ambient light conditions throughout the life cycle[1]. In *Arabidopsis thaliana*, phytochrome B (phyB) is predominantly involved in the regulation of R/FR light-dependent growth and development[2]. phyB exists in two reversible forms, biologically inactive (Pr) and biologically active (Pfr)[3]. A high R/FR ratio promotes the conversion of phyB from Pr to Pfr and subsequently triggers the translocation of phyB from the cytoplasm to the nucleus. Nucleus-localized phyB is assembled into discrete puncta known as photobodies (PBs), where it interacts with and promotes the degradation of PHYTOCHROME INTERACTING FACTORS (PIFs), resulting in developmental transition from skotomorphogenesis to photomorphogenesis[4–6]. Pfr can also be reverted to Pr via either FR light-dependent photoconversion or light-independent thermal reversion (also called dark reversion)[3].

[1]Shanghai Center for Plant Stress Biology, CAS Center for Excellence in Molecular Plant Sciences, Chinese Academy of Sciences, Shanghai, China. [2]University of the Chinese Academy of Sciences, Beijing, China. [3]Shanghai Key Laboratory of Plant Functional Genomics and Resources, Shanghai Chenshan Botanical Garden, Shanghai, China. [4]State Key Laboratory of Stem Cell and Reproductive Biology, Institute of Zoology, Chinese Academy of Sciences, Beijing, China. [5]Shanghai Bioprofile Technology Company Ltd, Shanghai, China. [6]Institute for Stem Cell and Regeneration, Chinese Academy of Sciences, Beijing, China. [7]Beijing Institute for Stem Cell and Regenerative Medicine, Beijing, China. [8]National Key Laboratory of Plant Molecular Genetics, CAS Center for Excellence in Molecular Plant Sciences, Institute of Plant Physiology and Ecology, Chinese Academy of Sciences, Shanghai, China. [9]Institute of Advanced Biotechnology and School of Life Sciences, Southern University of Science and Technology, Shenzhen, China. [10]Center for Advanced Bioindustry Technologies, Chinese Academy of Agricultural Sciences, Beijing, China. [11]Hainan Yazhou Bay Seed Laboratory, Sanya, China. e-mail: jkzhu@psc.ac.cn; czzhao@psc.ac.cn

The regulatory mechanisms underlying the activation and attenuation of phyB signalling have been extensively studied over the past two decades. After the absorption of light via bilin chromophores, the N-terminal domain of phyB is structurally changed, resulting in the exposure of the C-terminal nuclear localization signal and thus the trafficking of phyB to the nucleus[5,6]. Under dark conditions, however, phyB experiences a thermal reversion process that compromises light signalling. So far, several components that regulate the thermal reversion process have been identified, including PHOTOPERIODIC CONTROL OF HYPOCOTYL 1 (PCH1), ARABIDOPSIS RESPONSE REGULATOR4 (ARR4) and HEMERA (HMR)[7–11]. Phosphorylations of the N-terminal domain of phyB, including the Ser84, Ser86, Thr89-Thr91, Ser106 and Tyr104 sites, have been shown to be involved in the modulation of thermal reversion[12,13]. Abolishing the phosphorylation of these sites compromises thermal reversion, whereas phosphomimic mutations of these sites accelerate thermal reversion[12,13]. Although phosphorylation has been reported in several studies, the kinase(s) that phosphorylate(s) phyB is(are) still unknown and the biological significance of the phosphorylation-mediated regulation of thermal reversion is still poorly understood.

One of the typical phenotypes of a *phyB* mutant is an extended hypocotyl and petiole[14], indicating that phyB regulates cell growth in response to ambient light conditions. It has been shown that phyB-mediated signalling pathways are utilized by plants to regulate growth under stress conditions. For example, two independent studies reported that phyB acts as a thermosensor to regulate plant morphology under warm temperature conditions[15,16]. *phyB* mutation has also been shown to uncouple growth-defence trade-offs in plants[17]. As one of the major environmental stresses, high salinity severely affects plant growth and survival[18], and in some cases these adverse effects are aggravated under high light intensity. However, the molecular mechanisms underlying salt-induced growth inhibition and cell death are still largely unknown, and whether plants take advantage of the phyB-mediated light signalling pathways to regulate salt stress response remains to be determined.

FERONIA (FER) is a receptor-like kinase of the *Catharanthus roseus* receptor-like kinase 1-like (*Cr*RLK1L) family that harbours two extracellular malectin domains and a cytosolic kinase domain[19]. As a putative sensor of cell wall integrity, FER participates in the regulation of multiple biological processes, including fertilization, root hair growth, plant immunity and abiotic stress response[20–25]. Recently, we found that cell wall-localized leucine-rich repeat extensins (LRX) 3/4/5, rapid alkalinization factor (RALF) 22/23 and FER function as a module to regulate plant growth and salt tolerance by fine-tuning the homoeostasis of multiple phytohormones, including jasmonic acid (JA) and abscisic acid[26,27]. *lrx345* and *fer-4* mutants exhibit enhanced leaf bleaching under salt stress, but little is currently known about the molecular mechanisms underlying the leaf bleaching phenotype of these two mutants under salt stress. Here we found that *phyB* mutation suppresses both the dwarfism and salt-triggered leaf bleaching of the *lrx345* and *fer-4* mutants. FER directly interacts with and phosphorylates phyB, and disruption of phyB phosphorylation in *fer-4* mutant delays photobody dissociation and results in increased phyB protein abundance in the nucleus. Further studies indicate that the enhanced leaf bleaching phenotype of the *fer-4* mutant under salt stress is largely caused by the overaccumulation of phyB in the nucleus.

Results

Identification of *lrx345* suppressors under salt stress

To identify cellular components in the LRX3/4/5-RALFs-FER salt stress response pathway in *Arabidopsis*, we performed ethylmethane sulfonate-mediated mutagenesis in the *lrx345* mutant and screened for suppressors that exhibited a higher survival rate than the *lrx345* mutant under salt stress. Here we report one of these suppressors, *slrx620* (*suppressor of lrx345-620*), which exhibited a longer petiole and a higher survival rate under salt stress than the *lrx345* mutant (Extended Data Fig. 1a–d). The constitutively increased expression of JA-responsive genes *PDF1.2* and *PDF1.3* in the *lrx345* mutant was also attenuated by the *slrx620* mutation (Extended Data Fig. 1e).

To identify the mutated gene in the s*lrx620* that was responsible for the suppression of the *lrx345* mutant phenotypes, bulked segregant analysis (BSA) was conducted. The mapping result revealed an obvious peak at approximately 9 Mb on chromosome 2 (Extended Data Fig. 1f). By manually checking all the candidate mutations in this region, a nucleotide mutation (G1191A) was identified in the *phyB* gene that results in the change of tryptophan 397 to a premature stop codon (Extended Data Fig. 1g). Notably, similar to the phenotype of the *phyB* mutant[14], the *slrx620* mutant exhibited a long hypocotyl under white-light conditions (Extended Data Fig. 1h,i), which indicated that the *phyB* mutation was most likely responsible for the phenotypes of the *slrx620* mutant.

phyB mutation suppresses *lrx345* and *fer-4* phenotypes

We then crossed *phyB-9*, a widely used *phyB* mutant allele[14], with the *lrx345* and *fer-4* mutants. It is worth mentioning that *phyB-9* and *slrx620* share the same nucleotide mutation (G1191A) in the *phyB* gene. Similar to the *slrx620*, the leaf bleaching phenotype of the *lrx345* and *fer-4* mutants under salt stress was largely suppressed by the *phyB-9* mutation (Fig. 1a,b). Moreover, the reduced petiole length and the increased expression of JA-responsive genes *PDF1.2* and *PDF1.3* in the *lrx345* and *fer-4* mutants were all suppressed by the *phyB-9* mutation (Fig. 1c–e). Together, these results indicate that *phyB* mutation could rescue a wide range of the phenotypes of *lrx345* and *fer-4* mutants. However, our data showed that *phyB-9* mutation could not suppress the low fertility of the *fer-4* mutant (Extended Data Fig. 2a).

To validate that *phyB* mutation is responsible for suppressing the growth and salt-hypersensitive phenotypes of *fer-4* mutant, wild type (WT) *phyB* was transformed into *phyB-9 fer-4* double mutant. Phenotype analysis showed that ectopic expression of *phyB* restored the long petiole and salt-tolerant phenotypes of the *phyB-9 fer-4* double mutant to that of the *fer-4* mutant (Extended Data Fig. 2b–e). In addition, we found that overexpression of *phyB* in the wild-type background resulted in enhanced leaf bleaching under salt stress, which was similar to that observed in the *lrx345* and *fer-4* mutants (Extended Data Fig. 2f,g). It has been reported that the *fer-4* mutant displays a reduced plant height when grown on soil[22]. Here we found that *phyB* mutation suppressed the reduced plant height of the *fer-4* mutant, whereas overexpression of *phyB* in the *fer-4* mutant resulted in a more severe dwarf phenotype (Extended Data Fig. 2h,i).

Because the activity of phyB is affected by light intensity[28], we tested whether light intensity is a factor that determines the survival rate of the *lrx345* and *fer-4* mutants under high salinity. Indeed, these two mutants grown under weak white-light (WL) irradiance showed a much higher survival rate under salt stress than those grown under normal white-light (NL) conditions (Fig. 1f,g). As phyB is specifically involved in sensing red light, we then investigated whether the enhanced salt hypersensitivity of the *lrx345* and *fer-4* mutants under white-light conditions is specifically triggered by red light. To this end, the phenotypes of seedlings grown under monochromatic red light were examined. After red-light illumination, both *lrx345* and *fer-4* mutants exhibited enhanced leaf bleaching phenotype under salt stress (Extended Data Fig. 3a,b), and this phenotype was fully suppressed by *phyB* mutation (Extended Data Fig. 3a,b). In addition, the salt-triggered leaf bleaching phenotype of the *lrx345* and *fer-4* mutants was substantially improved under low red-light intensity compared with that under high red-light intensity (Extended Data Fig. 3c,d). Together, these data indicate that the phyB-mediated red-light signal is responsible for the leaf bleaching phenotype of the *lrx345* and *fer-4* mutants under salt stress.

https://doi.org/10.1038/s41477-023-01390-4

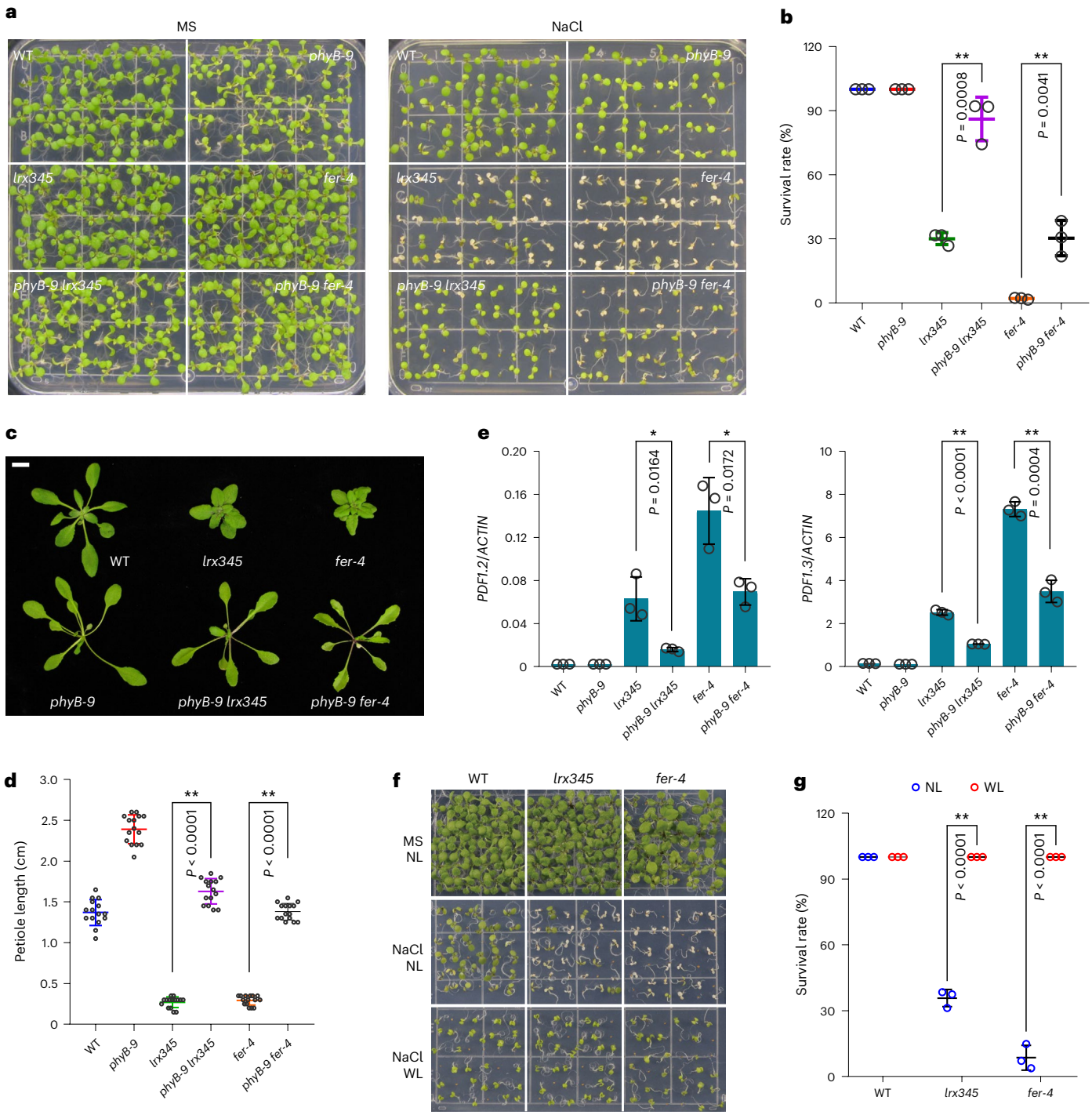

Fig. 1 | Mutation of *phyB* suppresses the phenotypes of *lrx345* and *fer-4* mutants. a, Phenotype of seedlings grown on 1/2 MS medium containing 0.8% agar and 1% sucrose (w/v) with or without NaCl (120 mM) under white-light (16 h light/8 h dark cycle) conditions. **b**, Survival rate of seedlings grown on NaCl medium for 8 d. The seedlings with full leaf bleaching were calculated as dead plants. Values are the means ± s.d. of three biological replicates. **c**, Representative images of each genotype grown on soils for 22 d under LD conditions (16 h light/8 h dark). Scale bar, 1 cm. **d**, The petiole length of the plants shown in **c**. Data are the means ± s.d. ($n = 15$ seedlings). **e**, RT–qPCR analysis of the transcript levels of *PDF1.2* and *PDF1.3* genes in each genotype. Values are the means ± s.d. of three biological replicates. **f**, Phenotypes of wild type, *lrx345* and *fer-4* mutants grown on 1/2 MS medium with or without NaCl (120 mM) under normal white light (NL, ~100 μmol m^{-2} s^{-1}) or weak white light (WL, ~5 μmol m^{-2} s^{-1}) in LD conditions. **g**, Survival rate of seedlings grown on NaCl medium as shown in **f**. Values are the means ± s.d. of three biological replicates. In **b**, **d**, **e** and **g**: $^{*}P < 0.05$, $^{**}P < 0.01$, two-sided Student's *t*-test.

To further understand the association of FER with phyB, RNA-seq assay was performed for the wild type, *fer-4* and *phyB-9 fer-4*. Transcriptome data revealed that 2,669 genes were constitutively upregulated in the *fer-4* mutant (fold change (FC) > 1.5, false discovery rate (FDR) < 0.05) (Supplementary Table 1), and among them, 272 exhibited reduced transcript levels in the *phyB-9 fer-4* mutant compared with the *fer-4* mutant (Extended Data Fig. 4a,b). Gene ontology (GO) enrichment analysis revealed that these 272 genes were enriched in the categories

of 'response to jasmonic acid', 'response to wounding' and 'response to salicylic acid' (Extended Data Fig. 4c), indicating that the constitutive activation of JA and SA signalling pathways in the *fer-4* mutant was attenuated by the *phyB* mutation. Previously, we reported that the enhanced leaf bleaching phenotype of the *lrx345* and *fer-4* mutants under high salinity is due to the overactivation of salt stress response and increased reactive oxygen species (ROS) accumulation[27]. Here, RNA-seq data showed that the above 272 genes were also enriched in the 'response to salt stress', 'response to oxidative stress' and 'response to ROS' categories (Extended Data Fig. 4c), suggesting that the *phyB* mutation compromised salt stress activation in the *fer-4* mutant. Among the 1,146 genes that were downregulated in the *fer-4* mutant (FC > 1.5, FDR < 0.05) (Supplementary Table 1), 135 showed significantly increased transcript levels in the *phyB-9 fer-4* mutant compared with the *fer-4* mutant (Extended Data Fig. 4d,e). GO enrichment analysis showed that 'response to auxin' and 'regulation of developmental growth' categories were enriched for these 135 genes (Extended Data Fig. 4f), indicating that phyB is involved in FER-mediated regulation of plant growth. Moreover, 57 genes belonging to the category of 'response to red or far-red light' were differentially expressed in the *fer-4* mutant compared with the wild type; among of them, 15 were restored in the *phyB-9 fer-4* mutant (FC > 1.5, FDR < 0.05), suggesting that FER participates in the regulation of red/far-red light response.

FER interacts with and phosphorylates phyB

To further understand the biological relationship between FER and phyB, we tested whether these two proteins are physically associated. FER is a plasma membrane-localized receptor-like kinase that harbours a cytoplasmic kinase domain (FERKD) (Fig. 2a). A yeast two-hybrid assay showed that FERKD interacted with full-length PHYB and the N-terminal region of PHYB (PHYBN), but not with the C-terminal region of PHYB (PHYBC) (Fig. 2b). A split luciferase complementation (split-LUC) assay performed in *Nicotiana benthamiana* further indicated that full-length phyB and phyBN, but not phyBC, interacted with both full-length FER and the cytosolic domain of FER (FERCD) (Fig. 2c). We then examined the interaction of FER with phyB in *Arabidopsis* using co-immunoprecipitation (Co-IP) assay. It is known that phyB is synthesized as an inactive Pr form in the cytosol and upon exposure to red light, Pr is rapidly converted to the active Pfr form and transported into the nucleus[6]. To investigate which form of phyB interacts with FER, seedlings were grown in darkness or exposed to red light before being subjected to Co-IP assay. The result showed that FER preferred to interact with the Pr form rather than the Pfr form of phyB (Fig. 2d). Consistent with this result, co-localization analysis indicated that, under dark conditions, FER and phyB were highly co-localized in the cytosol. Under white-light conditions, however, the majority of phyB were transported into the nucleus, while FER remained in the plasma membrane (Extended Data Fig. 5a). These results indicate that FER mainly interacts with the Pr form of phyB in the cytosol. A recent study showed that *Cr*RLK1L family members THE1 and HERK1 exhibit a similar function as FER in the regulation of salt tolerance[29]. Here, split-LUC assay showed that phyB also interacted with THE1, suggesting that multiple *Cr*RLK1L family proteins are probably involved in the regulation of the phyB signalling pathway (Extended Data Fig. 5b).

Because the cytosolic kinase domain of FER directly interacts with the N-terminal domain of phyB, we then tested whether FER may phosphorylate phyB. An in vitro kinase assay showed that FERCD was capable of phosphorylating phyBN (Fig. 2e). To verify the phosphorylation of phyBN by FER, mass spectrometry analysis was performed. In control samples with phyBN alone, a peak that matched the molecular weight of non-phosphorylated phyBN was identified (Extended Data Fig. 5c). Because phyBN was fused with an Avi-tag and this tag can bind to biotin, a peak representing the biotin-tagged non-phosphorylated phyBN was also identified in our mass spectrometry data (Extended Data Fig. 5c). In the sample incubated with FERCD, the abundance of non-phosphorylated phyBN was decreased, and two additional peaks next to the non-phosphorylated phyB peak appeared; the molecular weight of these two newly appeared peaks was increased by one and two phosphates, respectively (Extended Data Fig. 5c), suggesting that at least two residues of phyB were phosphorylated by FERCD. To validate the phosphorylation of phyB by FER in vivo, the phosphorylation level of phyB in the wild type and *fer-4* mutant was compared. Because FER predominantly interacts with the Pr form of phyB, etiolated seedlings grown under dark conditions were selected for the analysis of phyB phosphorylation. Immunoblotting assay was performed for immunoprecipitated phyB-GFP using anti-phosphoserine antibody, and the result showed that the phosphorylation level of phyB-GFP was dramatically reduced in the *fer-4* mutant (Fig. 2f).

To identify the phosphorylation sites, liquid chromatography–tandem mass spectrometry (LC–MS) analysis was performed for phyBN incubated with or without FERCD in vitro. Two residues, Ser106 and Ser227 (Fig. 2g and Extended Data Fig. 5d), were identified that exhibited increased phosphorylation levels in phyBN after incubation with FERCD. To verify that these two residues were the phosphorylation sites of phyB by FERCD, they were simultaneously mutated to Ala, and the mutated phyBN was subjected to in vitro kinase assay and LC–MS analysis. Both assays indicated that the phosphorylation level of phyBN^{S106AS227A} by FERCD was dramatically reduced (Fig. 2h and Extended Data Fig. 5c), corroborating that they were the major sites phosphorylated by FER. To verify the phosphorylation of these two residues in vivo, mass spectrometry analysis was performed in the wild type and *fer-4* mutant. In two independent biological replicates, the phosphorylation of both Ser106 and Ser227 was detected in the wild type (Extended Data Fig. 6a,b and Supplementary Table 2), demonstrating that they are the phosphorylation sites of phyB in planta. In the *fer-4* mutant, both Ser106 and Ser227 displayed reduced phosphorylation levels compared with that in the wild type (Extended Data Fig. 6c,d), indicating that FER is required for the phosphorylation of these two residues in vivo. In a previous study, it was shown that phosphorylation of Ser86 is required for the regulation of thermal reversion[12], but the kinase that phosphorylates this residue is still unknown. Our data showed that mutation of Ser86 to Ala did not affect the phosphorylation of phyBN by FERCD (Extended Data Fig. 5e), suggesting that additional kinase(s) rather than FER phosphorylate(s) Ser86.

Dark-induced photobody dissociation is delayed in *fer-4*

To investigate the biological relevance of FER-mediated phosphorylation of phyB, the protein abundance of phyB was examined using an antibody against endogenous phyB. The phyB protein abundance was slightly increased in the *lrx345* and *fer-4* mutants compared with that in the wild type (Fig. 3a). The phosphorylation of phyB has been implicated in the regulation of photobody assembly and dissociation[12,13], so we investigated whether *fer-4* mutation may affect photobody dynamics. Under our growth conditions, we found that after white-light illumination for 5 h (Zeitgeber time 5, ZT5), majority of phyB proteins had aggregated into photobodies in both the wild type and *fer-4* mutant, so we chose ZT5 as a time point to perform photobody dynamics analysis. Five-day-old seedlings of the wild type and *fer-4* mutant grown under a 16 h light/8 h dark cycle were exposed to white light for 5 h (ZT5) after dawn and then subjected to continuous dark conditions. At ZT5, the size of the photobodies was comparable between these two genotypes (Fig. 3b,c). After dark treatment for 1 h and 3 h, the photobodies gradually disassembled in both the wild type and *fer-4* mutant, but the *fer-4* mutant exhibited a much slower rate of photobody dissociation (Fig. 3b,c), suggesting that *fer-4* mutation leads to enhanced photobody stability under dark conditions.

To understand whether *fer-4* mutation also affects the protein abundance of phyB in the nucleus, we performed a nuclear fractionation assay. Six-day-old seedlings grown under long-day conditions (16 h light/8 h dark) were collected at ZT5 after dawn, and the proteins from cytosolic and nuclear fractions were separated. Immunoblotting

https://doi.org/10.1038/s41477-023-01390-4

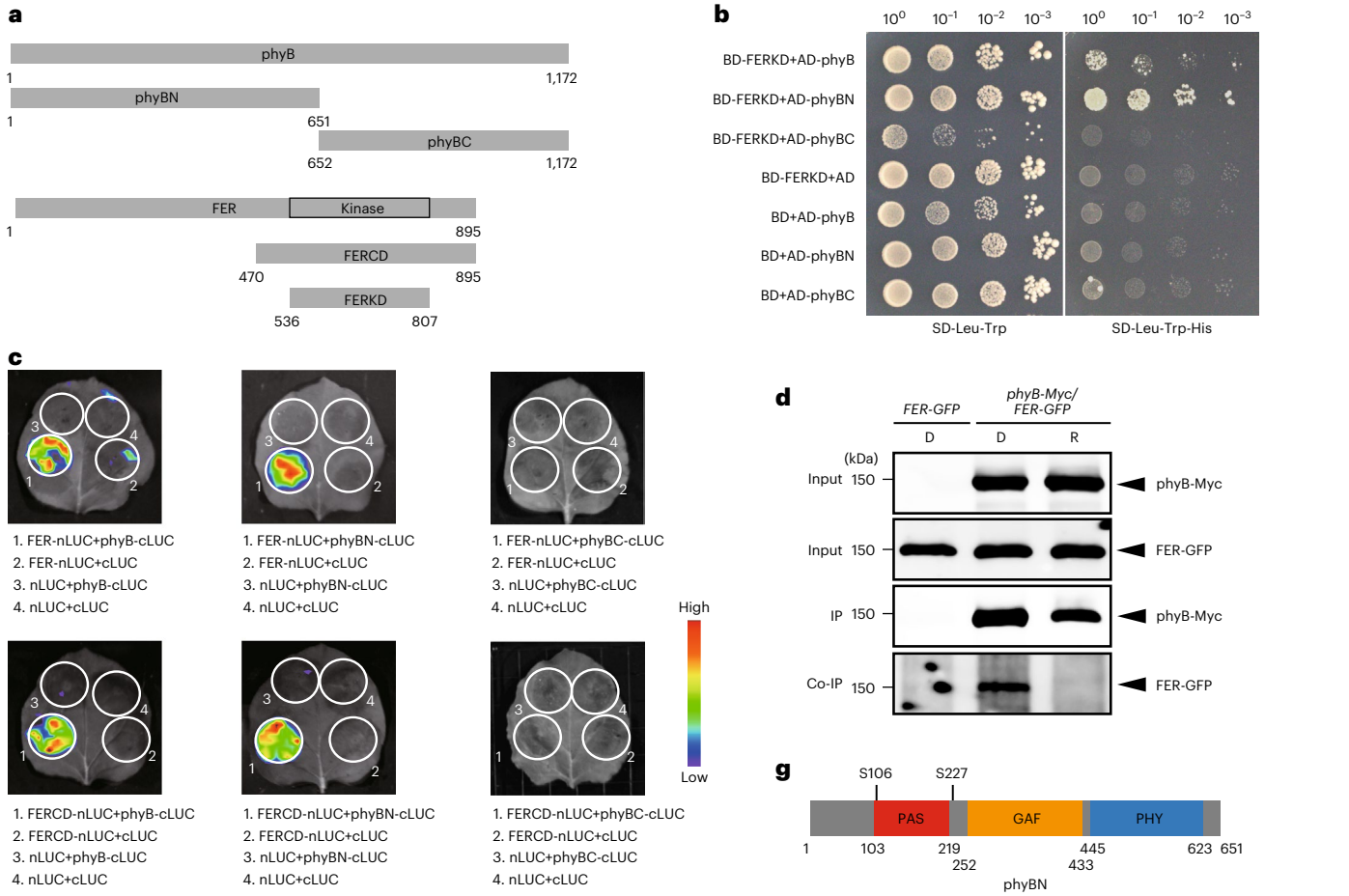

Fig. 2 | FER interacts with and phosphorylates the N-terminal domain of phyB. a, Schematic illustration of the protein structure of phyB and FER. The numbers indicate the position of each protein domain. **b**, A yeast two-hybrid assay was performed to test the interaction between FER and phyB. Yeast cells carrying the indicated constructs were grown on SD/-Trp/-Leu or SD/-Trp/-Leu/-His medium. **c**, Split luciferase complementation assays showing the interaction of FER or FERCD with each phyB variant. Fluorescence was detected at 48 h after infiltration of the indicated constructs. **d**, Co-immunoprecipitation was performed to test the interaction of FER with phyB in vivo. Total proteins were extracted from 7-day-old etiolated seedlings grown in darkness or exposed to red light for 6 h. phyB-Myc proteins were immunoprecipitated using anti-Myc antibody. Immunoblottings were performed using anti-Myc and anti-GFP antibodies. **e**, Analysis of the phosphorylation of phyBN by FERCD using an in vitro kinase assay. Top: phosphorylated proteins were detected by immunoblotting using anti-thiophosphate ester antibody. Bottom: recombinant phyBN and FERCD were detected by CBB staining. **f**, Analysis of the phosphorylation of phyB by FER in vivo. Total proteins were extracted from 7-day-old etiolated seedlings grown in continuous darkness. phyB-GFP protein was immunoprecipitated by incubating with anti-GFP magarose beads. Immunoblottings were performed using anti-phosphoserine and anti-GFP antibodies. **g**, Schematic illustration of the phosphorylation sites of phyBN by FERCD identified by LC–MS. **h**, In vitro kinase assay showing the phosphorylation of phyBN^{WT} and phyBN^{S106AS227A} by FERCD. The experiments in **d**, **e**, **f** and **h** were repeated independently at least three times with similar results.

assays showed that the protein abundance of phyB in the nucleus was largely increased in the *fer-4* mutant compared with that in the wild type (Fig. 3d). During our study, we noted that total phyB protein level was substantially increased in seedlings after dark treatment for 3 d, but the phyB protein in the nucleus was dramatically decreased (Fig. 3d), implying the possibility of trafficking of phyB from the nucleus to the cytosol after prolonged exposure to dark conditions. We then tested whether FER is required for modulating phyB protein abundance in the nucleus after prolonged dark treatment. Compared with the wild type, the protein abundance of phyB in the nucleus retained a high level in the *fer-4* mutant after dark treatment for 3 d (Fig. 3d). Together, these results indicate that FER negatively regulates the protein abundance of phyB in the nucleus. In agreement with this notion, dark-induced hypocotyl elongation was largely compromised in the *fer-4* mutant and this growth inhibition was restored by the *phyB* mutation (Fig. 3e,f). In addition, we measured fluence rate response curves of hypocotyl

https://doi.org/10.1038/s41477-023-01390-4

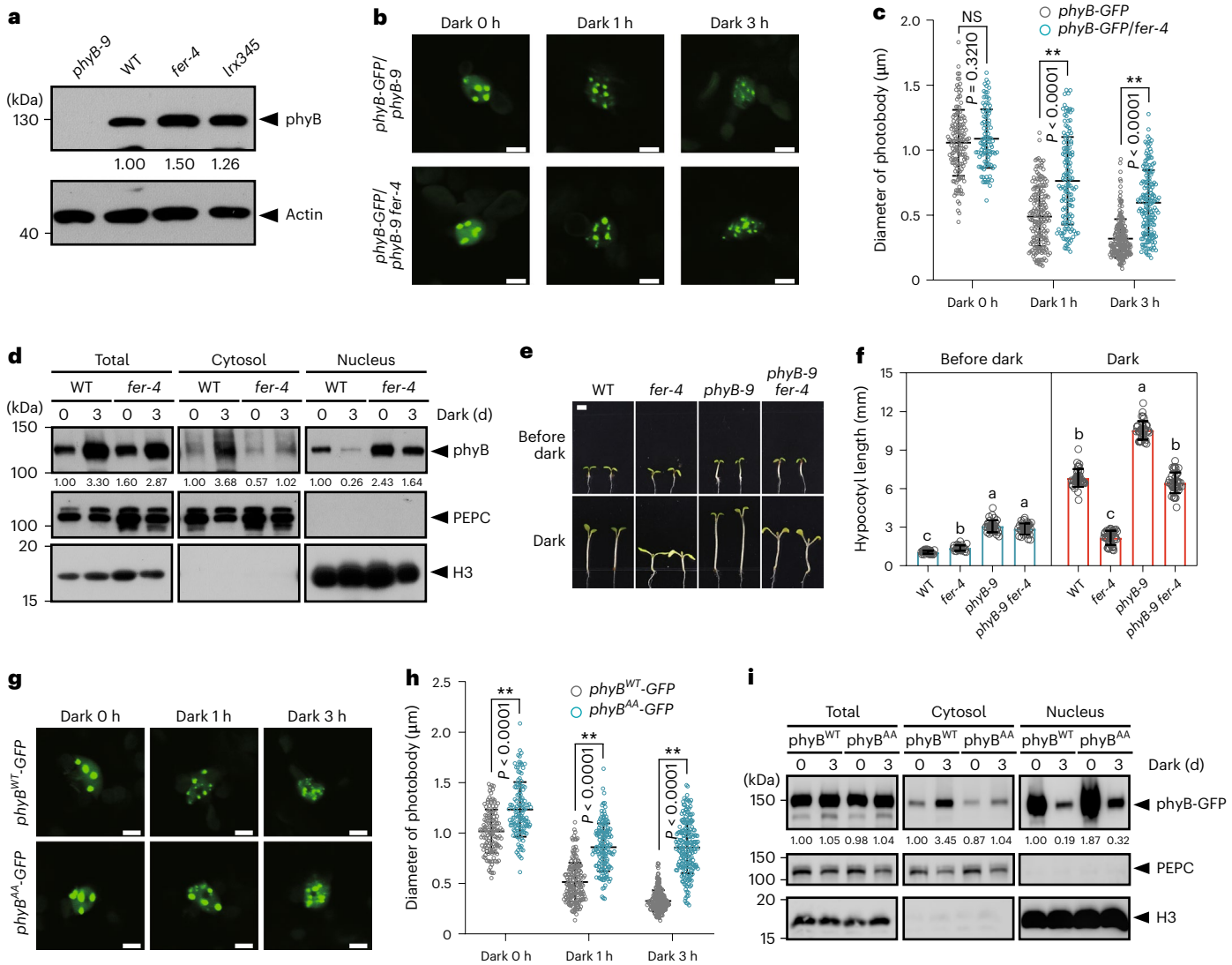

Fig. 3 | FER-mediated phosphorylation controls photobody dissociation and phyB protein abundance in the nucleus. a, Comparison of phyB protein abundance in 8-day-old seedlings using anti-phyB and anti-actin antibodies. **b**, Photobody dissociation was detected under dark conditions. Five-day-old seedlings were exposed to white light for 5 h (ZT5) after dawn, and then photobodies in the cotyledons were detected after dark treatment for 0, 1 and 3 h. Scale bar, 4 μm. **c**, Quantification of the diameter of phyB photobodies shown in **b**. Values are the means ± s.d. ($n > 100$ bodies from 30–40 cells). NS, not significant. **d**, Nuclear fractionation assay was performed to analyse phyB abundance in the nucleus. Six-day-old seedlings at ZT5 (defined as 0 day) and seedlings grown in darkness for an additional 3 d were collected for protein extraction and immunoblotting assays. PEPC and H3 were used as cytosolic and nuclear markers, respectively. Band abundance was estimated using ImageJ, and in each fractionation, the value of the wild-type sample at 0 day was set as 1. **e**, Hypocotyl growth of seedlings in darkness. Four-day-old seedlings grown under LD conditions were transferred to dark conditions. Pictures were photographed before (top) and after dark treatment for 3 d (bottom). Scale bar, 2 mm. **f**, Quantification of the hypocotyl length of the seedlings shown in **e**. Values are the means ± s.d. ($n > 35$ seedlings). **g**, Comparison of photobody dissociation in the cotyledons of *phyB*^{WT}*-GFP*/*phyB-9* and *phyB*^{AA}/*phyB-9#3* transgenic plants. The experiment was performed using a similar procedure as in **b**. AA represents S106A and S227A mutations. Scale bar, 4 μm. **h**, Quantification of the diameter of phyB photobodies shown in **g**. Values are the means ± s.d. ($n > 100$ bodies from 30–40 cells). **i**, Nuclear fractionation assay was performed to analyse phyB abundance in the nucleus of *phyB*^{WT}*-GFP*/*phyB-9* and *phyB*^{AA}/*phyB-9#3* transgenic plants. In **c** and **h**, $^{**}P < 0.01$, two-sided Student's *t*-test. Different letters in **f** indicate statistically significant differences ($P < 0.01$, one-way ANOVA). The experiments in **a**, **d** and **i** were repeated independently at least twice with similar results.

lengths under different fluence rates of red light. The *fer-4* mutant exhibited a shorter hypocotyl than the wild type when grown at low fluence rates (0.85 and 2.7 μmol m^{-2} s^{-1}), but they exhibited a similar response at higher fluence rates (6 and 9 μmol m^{-2} s^{-1}) (Extended Data Fig. 3e). This result suggested that the *fer-4* mutation led to an increased response to red light, especially under low red-light fluence rates.

Phosphorylation of phyB promotes photobody dissociation

To determine whether the phospho-mutated phyB was more stable in the photobody under dark conditions, transgenic plants expressing *phyB*^{WT} and *phyB*^{S106AS227A} in the *phyB-9* mutant background were generated, and the transgenic plants with similar phyB protein abundance were collected for the analysis of photobody (Extended Data Fig. 7a). At ZT5, the phyB protein aggregated into photobodies in both the *phyB*^{WT}/*phyB-9* and *phyB*^{S106AS227A}/*phyB-9* seedlings. After dark treatment, phyB^{S106AS227A} showed a much slower photobody dissociation rate than the wild-type phyB (Fig. 3g,h), suggesting that phosphorylations negatively regulate photobody stability under dark conditions. We also performed nuclear fractionation assay to compare nuclear phyB abundance between *phyB*^{WT}/*phyB-9* and *phyB*^{S106AS227A}/*phyB-9*

transgenic plants, and found that substitution of Ser106 and Ser227 to Ala resulted in increased phyB protein abundance in the nucleus compared with the phyB^{WT} both before and after dark treatment (Fig. 3i), which was similar to that observed in the *fer-4* mutant. Notably, the elevation of endogenous phyB protein abundance after dark treatment for 3 d was not obviously detected for ectopically expressed phyB-GFP under the control of cauliflower mosaic virus (CaMV) 35S promoter (Fig. 3i), implying that transcriptional regulation might be involved in the control of phyB protein abundance under continuous dark conditions.

Phenotype analysis indicated that both the *phyB^{WT}* and *phyB-^{S106AS227A}* transgenes complemented the long hypocotyl phenotype of the *phyB-9* mutant under white-light conditions. Because the growth inhibition response in *phyB^{WT}*-overexpressing plants was almost saturated, it was difficult to distinguish the difference between *phyB^{WT}*/*phyB-9* and *phyB^{S106AS227A}*/*phyB-9* transgenic plants in terms of hypocotyl elongation under long-day (16 h light/8 h dark cycle) conditions (Extended Data Fig. 7b,c). We then analysed the hypocotyl elongation of the seedlings after they were transferred from white light to continuous dark conditions, and found that the dark-induced hypocotyl elongation in the *phyB^{S106AS227A}*/*phyB-9* transgenic plants was slower than that of the *phyB^{WT}*/*phyB-9* transgenic plants (Extended Data Fig. 7d), suggesting that substitutions of Ser106 and Ser227 to Ala enhance the biological function of phyB.

We also generated transgenic plants expressing *phyB^{S106DS227D}-GFP* in the *phyB-9* mutant, and the transgenic lines with similar phyB protein abundance as *phyB^{WT}-GFP* were chosen for the analysis of photobody behaviour (Extended Data Fig. 7e). We found that photobody size in *phyB^{S106DS227D}-GFP* transgenic plants was smaller than that in *phyB^{WT}-GFP* transgenic plants both before and after dark treatment (Extended Data Fig. 7f,g), corroborating that phosphorylation negatively regulates photobody stability. Using the same transgenic lines, we found that *phyB^{S106DS227D}* could fully complement the hypocotyl elongation phenotype of the *phyB-9* mutant (Extended Data Fig. 7h). Given that phyB-mediated signalling output is tightly correlated with its protein abundance in the nucleus[30], we speculated that complete rescue of the *phyB-9* mutant phenotype by the *phyB^{S106DS227D}* was probably due to the high protein abundance of *phyB^{S106DS227D}*. We then selected three independent transgenic lines that exhibited a relatively low phyB^{S106DS227D}-GFP protein level, but the protein abundance in these transgenic lines was still much higher than the endogenous phyB protein abundance (Extended Data Fig. 7i). Phenotype analysis showed that *phyB^{S106DS227D}* only partially complemented the long hypocotyl phenotype of the *phyB-9* mutant (Extended Data Fig. 7j,k), suggesting that phyB activity is compromised when Ser106 and Ser227 are constitutively phosphorylated.

FER accelerates dark-induced Pfr-to-Pr conversion in vitro

The photobody dissociation under dark conditions is usually accompanied by the conversion of Pfr to Pr[6], so the effect of phosphorylation on the photoswitching of phyB was analysed. As reported previously[31], phyBN displayed two peaks at 651 nm (Pr form) and 714 nm (Pfr form) after red-light illumination, and Pfr was successfully converted to Pr after far-red light irradiance for 5 min (Extended Data Fig. 8a,b), suggesting that the purified phyBN functions well in light absorption in vitro. We then examined the role of FER in the regulation of dark-triggered Pfr-to-Pr conversion. The phyBN protein was exposed to red-light illumination for 5 min before being subjected to dark treatment. For the sample with phyBN protein alone, Pfr/Pr ratio was gradually reduced after dark treatment. Addition of FERCD, however, triggered the phosphorylation of phyBN and greatly accelerated the conversion of Pfr to Pr (Fig. 4a,b). As a control, FERCD^{K565R}, a kinase-dead form of FERCD, was not able to phosphorylate phyBN and thus could not accelerate Pfr-to-Pr conversion under dark conditions (Fig. 4a,b). It should be noted that the protein size of FERCD^{K565R} is smaller than that of FERCD^{WT} on sodium dodecyl sulphate-polyacrylamide gel electrophoresis (SDS–PAGE), which is probably caused by the absence of autophosphorylation due to disrupted kinase activity. This is supported by the result showing that the FERCD^{WT} treated with λPPase exhibited a similar protein size as FERCD^{K565R} (Extended Data Fig. 8c). Together, these results suggested that FER-mediated phosphorylation was sufficient to promote Pfr-to-Pr conversion under dark conditions.

The Pfr-to-Pr conversion of each phospho-mutated phyB with similar protein abundance was also analysed (Fig. 4c), which showed that phyBN^{S106AS227A} exhibited delayed reversion from Pfr to Pr under dark conditions compared with the phyBN^{WT} (Fig. 4d). Our results verified that substitution of Ser86 to Ala delayed Pfr-to-Pr conversion under dark conditions as reported previously[12]. Remarkably, simultaneous substitutions of Ser86, Ser106 and Ser227 to Ala (phyBN^{AAA}) almost fully abolished Pfr-to-Pr reversion under dark conditions (Fig. 4d), indicating that these three residues were the major phosphorylation sites contributing to the regulation of dark-triggered Pfr-to-Pr reversion. In contrast, far-red light-triggered photoconversion was not affected in these phospho-mutated phyBN (Extended Data Fig. 8a,b), indicating that phosphorylation is mainly required for the regulation of Pfr-to-Pr reversion under dark conditions.

Salt stress slows down photobody dissociation

Suppression of the salt hypersensitivity of the *fer-4* mutant by the *phyB* mutation suggested that phyB participates in the regulation of salt stress response. To analyse photobody dissociation under salt stress, 5-day-old *phyB-GFP^{WT}* seedlings grown under a 16 h light/8 h dark cycle were transferred to MS media supplemented with or without NaCl at ZT0, and then the seedlings were exposed to white light for 5 h (ZT5) before being subjected to dark treatment for 1 and 3 h. The results showed that the dark-triggered dissociation of photobodies was substantially delayed in the seedlings grown on salt medium (Fig. 5a,b), indicating that salt stress enhanced the stability of the photobody. Using a similar treatment procedure as described above for photobody analysis, we examined the effect of salt stress on the protein abundance of phyB in the nucleus. After being transferred to salt medium for 5 h under white-light conditions, the seedlings showed a higher phyB protein level in the nucleus than those grown on MS medium (Fig. 5c), suggesting that salt stress may enhance nuclear phyB protein stability even under white-light conditions. After dark treatment for 3 d, phyB protein abundance in the nucleus was largely reduced in the wild type grown on MS medium, but salt stress substantially compromised dark-triggered phyB protein reduction in the nucleus (Fig. 5c). These results indicate that salt stress promotes the accumulation of phyB in the nucleus, which is similar to that observed in the *fer-4* mutant.

Because salt stress and *fer-4* mutation had a similar effect on the behaviours of phyB, we speculated that salt stress might negatively regulate the activity of FER. Immunoblotting assays showed that the protein level of FER was not affected after NaCl treatment (Fig. 5d). We then examined the kinase activity of FER by using an IP-kinase assay. The *FER-GFP* transgenic plants were treated with NaCl or H_2O and the immunoprecipitated FER-GFP was subjected to kinase reactions. The results showed that the autophosphorylation of FER was largely compromised by NaCl treatment but not by H_2O treatment (Fig. 5e), suggesting that salt stress inhibits the kinase activity of FER. Immunoblotting assay using anti-phosphoserine antibody showed that the phosphorylation of phyB was only slightly reduced in the wild type but not reduced in the *fer-4* mutant after salt treatment (Extended Data Fig. 6e). Because there are a lot of phosphorylation sites in phyB[13], and anti-phosphoserine antibody potentially recognizes all the phosphorylated Ser or Thr in phyB, the intensity of the phosphorylation band in SDS–PAGE could not accurately reflect the phosphorylation level of specific residues. We then analysed the phosphorylation of phyB under salt stress using mass spectrometry analysis, which can recognize the phosphorylation of specific residues, and found that the phosphorylation level of Ser106 was significantly reduced in the wild-type plants after salt treatment

https://doi.org/10.1038/s41477-023-01390-4

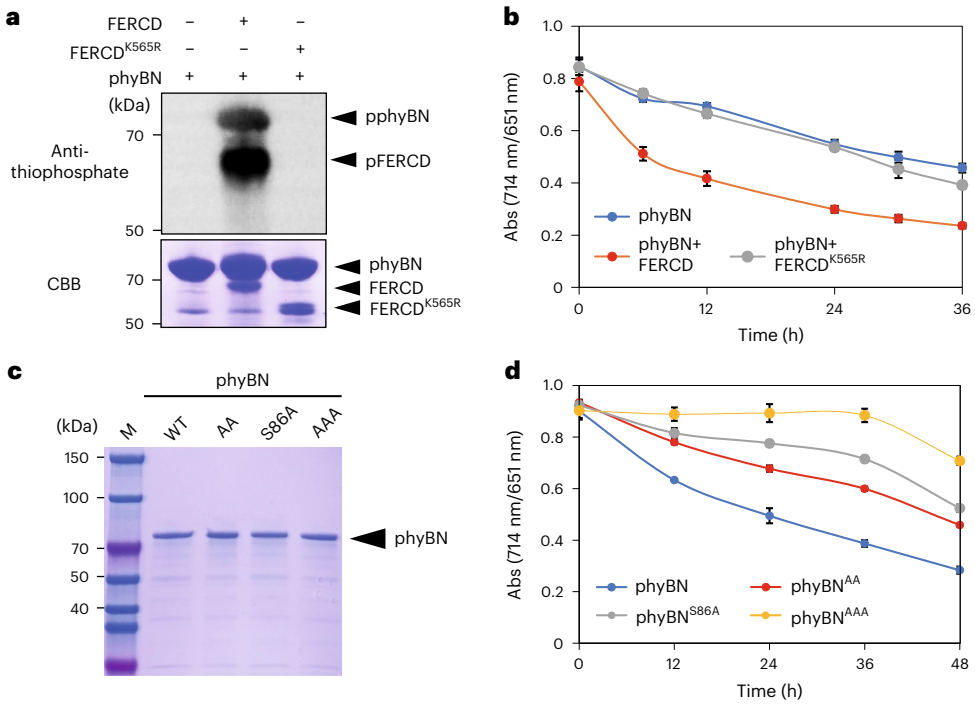

Fig. 4 | FER-mediated phosphorylation of phyB accelerates the dark-triggered Pfr-to-Pr conversion in vitro. a, Analysis of the phosphorylation of phyBN by FERCD and FERCD^{K565R} using an in vitro kinase assay. Top: phosphorylated proteins were detected by immunoblotting using anti-thiophosphate ester antibodies. Bottom: recombinant phyBN, FERCD and FERCD^{K565R} are indicated by CBB staining. **b**, Spectral analysis of the photoswitching of phyBN after incubation in a kinase reaction buffer with or without FERCD. After illumination with red light (660 nm, ~17 μmol m^{-2} s^{-1}) for 5 min, the phyBN proteins (PCB was used as chromophore) were transferred to dark conditions and absorption spectra were measured. The kinase-dead version of FERCD (FERCD^{K565R}) was used as a control. The *y* axis represents the Pfr/Pr ratio. **c**, CBB staining showing recombinant phyBN, phyBN^{S106AS227A} (AA), phyBN^{S86A} (S86A) and phyBN^{S86AS106AS227A} (AAA). **d**, Spectral analysis of the Pfr-to-Pr conversion of each phyBN variant after dark treatment. The experiment was performed using a similar procedure as in **b**. Values in **b** and **d** are the means ± s.d. of three biological replicates.

(Extended Data Fig. 6f). On the basis of these results, we propose that salt stress inhibits the kinase activity of FER and thus affects the phosphorylation of phyB.

phyB mutation improves salt tolerance in *Arabidopsis* and rice

Since phyB plays an important role in the regulation of hypocotyl elongation, we tested whether the salt-induced inhibition of hypocotyl growth depends on phyB-mediated pathways. On MS medium, the wild type and *phyB-9* mutant exhibited a similar hypocotyl length after growth under dark conditions for 5 d. Under salt stress, hypocotyl elongation was dramatically inhibited in the wild type, while this inhibition was partially alleviated in the *phyB-9* mutant (Fig. 5f,g), suggesting that the salt-induced inhibition of hypocotyl elongation partially depends on phyB.

To understand whether the increased leaf bleaching phenotype of the *fer-4* mutant under salt stress was correlated with the increased accumulation of phyB in the nucleus, we observed the phenotype of *YHB* plants under salt stress. The *YHB* plant harbours a Y276H mutation in phyB that leads to the constitutive localization of phyB in the nucleus[32]. Similar to the *fer-4* mutant, the *YHB* plants displayed an enhanced leaf bleaching phenotype under salt stress (Fig. 5h,i), supporting the idea that the increased accumulation of phyB in the nucleus was responsible for the reduced survival rate of plants under salt stress. This notion was also supported by the results showing that overexpression of *phyB*^{WT} in the *phyB-9* mutant resulted in enhanced leaf bleaching, while overexpression of *phyB*^{S106AS227A} caused an even more severe phenotype under salt stress (Extended Data Fig. 9a). To test whether phyB is also involved in the regulation of salt tolerance in other plant species, we analysed the phenotype of the *OsphyB* mutant in rice (*Oryza sativa*) under salt stress. Strikingly, the *OsphyB* mutant exhibited a substantially higher survival rate than the wild-type plants (Fig. 5j,k), verifying that disruption of phyB is beneficial for the survival of plants under salt stress.

PIF5 overexpression suppresses *lrx345* and *fer-4* phenotypes

PIFs are transcription factors that function downstream of phyB to regulate photomorphogenesis[6]. As the *phyB* mutation suppressed the dwarfism and salt hypersensitivity of the *lrx345* and *fer-4* mutants, we wondered whether PIFs are involved in the LRX3/4/5-FER module-mediated regulation of plant growth and salt tolerance. Consistent with the increased accumulation of phyB in the nucleus, *PIF5-YFP* transgenic plants in the *lrx345* and *fer-4* backgrounds showed substantially lower PIF5 protein abundance than in the wild type (Fig. 6a), although the transcript level of *PIF5* was similar in these transgenic plants (Extended Data Fig. 9b). Treatment of plants with MG132, an inhibitor of 26S proteasome, substantially increased the protein level of PIF5 in the *lrx345* and *fer-4* mutants (Fig. 6a), indicating that the reduction of PIF5 in these two mutants was caused by 26S proteasome-mediated degradation. As a direct target of phyB, the reduced PIF5 protein abundance in the *lrx345* and *fer-4* mutants was fully recovered by the *phyB* mutation (Fig. 6b).

Consistent with the finding that salt stress promoted the stability of phyB in the nucleus, the PIF5 protein abundance in the wild type was gradually reduced under salt stress. However, in the *lrx345* and *fer-4* mutants, salt stress-triggered degradation of PIF5 was completely abolished (Fig. 6c). Moreover, salt stress-induced degradation of PIF5 was compromised in the *phyB-9* mutant (Fig. 6d), indicating that phyB acts upstream of PIFs in response to salt stress. Notably, these salt treatment

https://doi.org/10.1038/s41477-023-01390-4

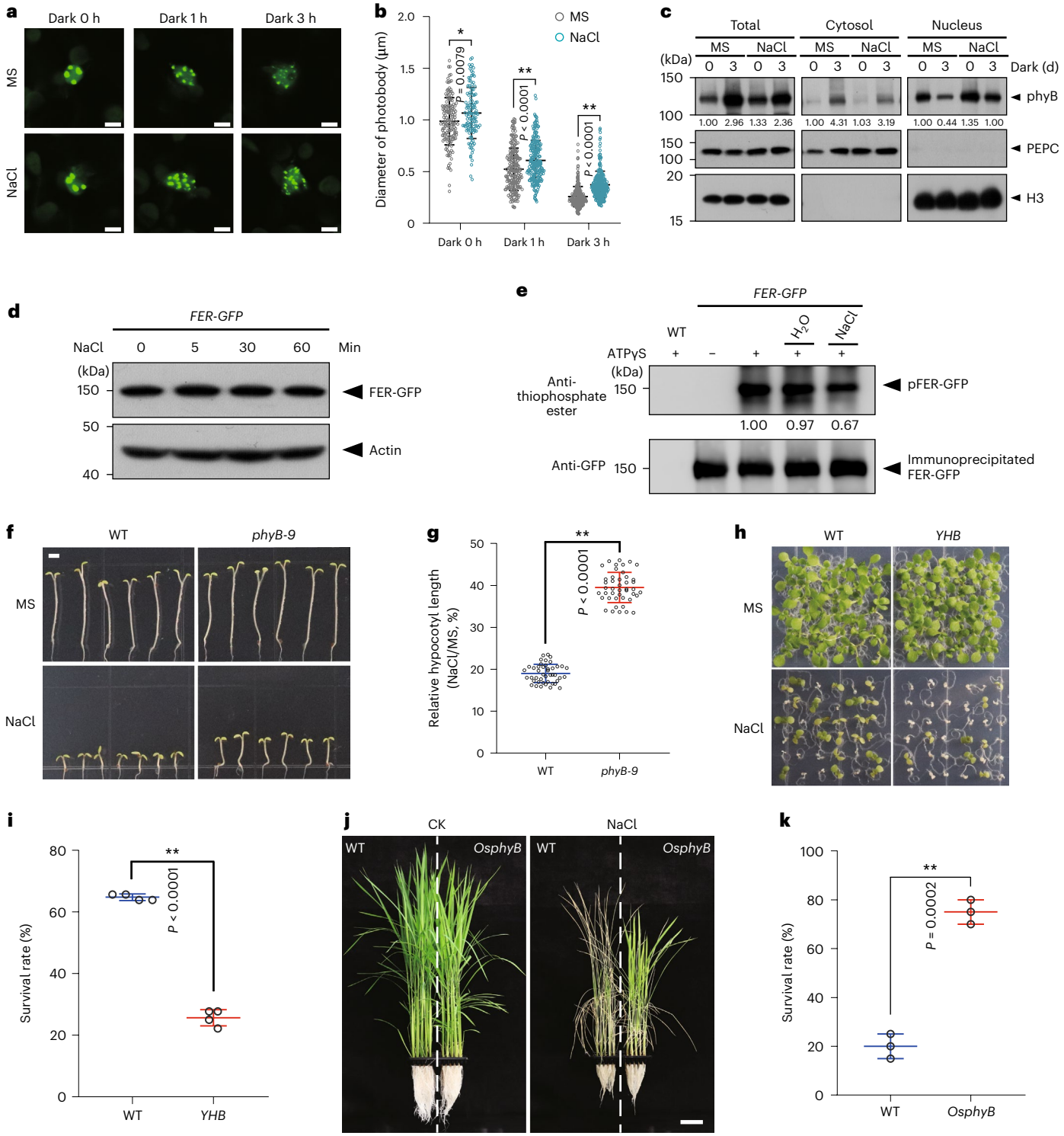

Fig. 5 | Salt stress delays photobody dissociation and increases phyB protein abundance in the nucleus via the inactivation of FER. a, Analysis of photobody dissociation under salt stress. Five-day-old *35S::phyB^{WT}-GFP/phyB-9* seedlings were transferred to 1/2 MS or NaCl (130 mM) medium at ZT0, and the seedlings at ZT5 were transferred to darkness for 1 h and 3 h. Scale bar, 4 μm. **b**, Quantification of the diameter of phyB photobodies shown in **a**. Values are the means ± s.d. (n > 100 bodies from 30–40 cells). **c**, Comparison of phyB abundance in the nucleus with or without salt treatment. Six-day-old wild-type seedlings were transferred to 1/2 MS or NaCl (150 mM) medium at ZT0, and then the seedlings were collected at ZT5 (defined as 0) or after growth in darkness for an additional 3 d (defined as 3) before immunoblotting assays. **d**, Analysis of FER-GFP protein abundance after NaCl (150 mM) treatment. **e**, Analysis of FER kinase activity after treatment with H_2O or NaCl (150 mM) for 5 min. Autophosphorylation of FER was examined using anti-thiophosphate ester antibody. **f**, Hypocotyl phenotype of 3-day-old seedlings after being transferred to 1/2 MS or NaCl (120 mM) medium and grown in darkness for 5 d. Scale bar, 2 mm. **g**, Relative hypocotyl length of seedlings shown in **f**. Values are the means ± s.d. (n > 20 seedlings). **h**, Phenotypes of seedlings grown on 1/2 MS or NaCl (120 mM) medium under white-light conditions (16 h light/8 h dark cycle). **i**, Survival rate of seedlings grown on salt medium. Values are the means ± s.d. (n = 4). **j**, Phenotypes of wild-type Nipponbare and *OsphyB* mutant plants after treatment with or without 100 mM NaCl for 12 d. Scale bar, 5 cm. **k**. Quantification of the survival rate of plants after salt treatment. Values are the means ± s.d. of three biological replicates (n = 20 seedlings). In **b**, **g**, **i** and **k**: *P < 0.05, **P < 0.01, two-sided Student's t-test. The experiments in **c**–**e** were repeated independently at least twice with similar results.

https://doi.org/10.1038/s41477-023-01390-4

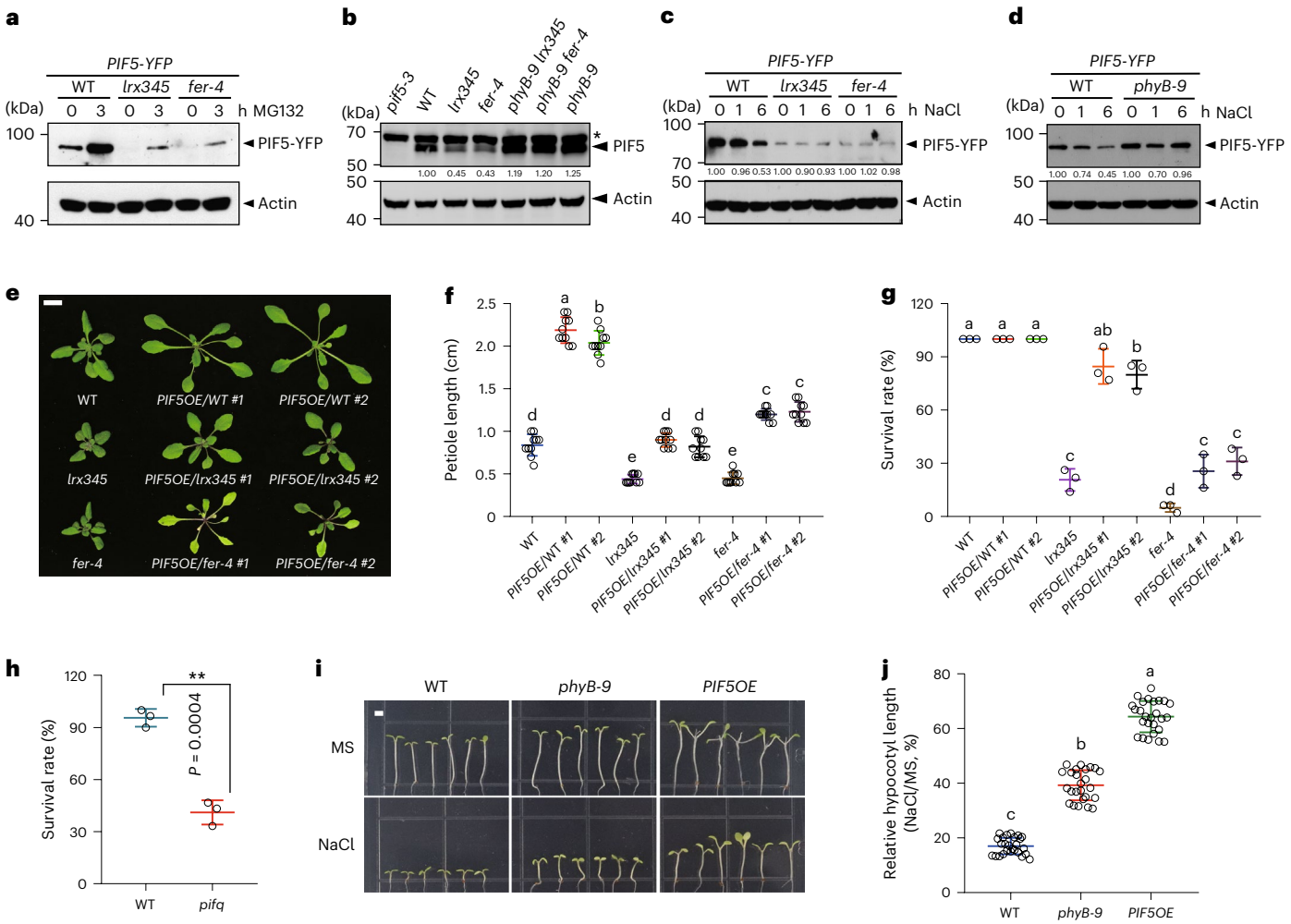

Fig. 6 | Overexpression of *PIF5* suppresses the phenotypes of *lrx345* and *fer-4* mutants. a, Analysis of PIF5 protein abundance in each genotype. Eight-day-old seedlings were treated with 50 μM MG132 or dimethyl sulfoxide for 3 h before immunoblotting assay using anti-GFP antibody. **b**, Analysis of PIF5 protein abundance in each genotype. Total protein was extracted from 8-day-old seedlings and immunoblotting was performed using anti-PIF5 antibody. Asterisk indicates a non-specific band. **c**, Analysis of PIF5-YFP protein abundance before and after NaCl treatment. Eight-day-old seedlings were treated with 150 mM NaCl under white-light conditions and immunoblotting was performed using anti-GFP antibody. **d**, Analysis of PIF5-YFP protein abundance in the wild type and *phyB-9* mutant background before and after 150 mM NaCl treatment under white-light conditions. Immunoblotting was performed using anti-GFP antibody. **e**, Representative images of each genotype grown on soils for 22 d under LD conditions. Scale bar, 1 cm. **f**, Quantification of the petiole length of plants shown in **e**. Values are the means ± s.d. ($n = 15$ seedlings). **g**, Survival rate of seedlings grown on NaCl (120 mM) medium under white light in LD conditions. Values are the means ± s.d. of three biological replicates. **h**, Survival rate of seedlings grown on NaCl (120 mM) medium under white-light conditions (16 h light/8 h dark cycle). Values are the means ± s.d. of three biological replicates ($n = 30$ seedlings in each replicate). **i**, Hypocotyl phenotype of each genotype. Three-day-old seedlings were transferred to 1/2 MS or NaCl (120 mM) medium and grown under dark conditions for 5 d. Scale bar, 2 mm. **j**, Relative hypocotyl length of seedlings grown on NaCl medium compared with those grown on MS medium under dark conditions. Values are the means ± s.d. ($n = 25$ seedlings). Different letters in **f**, **g** and **j** indicate statistically significant differences ($P < 0.01$, one-way ANOVA). In **h**, $^{**}P < 0.01$, two-sided Student's *t*-test. The experiments in **a**–**d** were repeated independently at least three times with similar results.

experiments were performed under white-light conditions, suggesting that salt stress may also affect phyB behaviour under white-light conditions. This conclusion can be supported by our immunoblotting assay showing that salt stress increased the protein abundance of phyB in the nucleus under white-light conditions (Fig. 5c).

Similar to the *phyB-9* mutation, overexpression of *PIF5* rescued the dwarfism and salt-induced leaf bleaching of the *lrx345* and *fer-4* mutants (Fig. 6e–g). Moreover, overexpression of *PIF3* also largely rescued the leaf bleaching phenotype of the *fer-4* mutant under salt stress (Extended Data Fig. 9c–e). These results suggest that suppression of the mutant phenotypes of *lrx345* and *fer-4* by *phyB* mutation depends on the accumulation of PIF proteins. In addition, we found that *pifq*, in which *PIF1*, *PIF3*, *PIF4* and *PIF5* genes are all absent, displayed a lower survival rate compared with the wild type under salt stress (Fig. 6h), further supporting the involvement of PIFs in the regulation of salt tolerance. Remarkably, salt-induced hypocotyl elongation inhibition was dramatically attenuated in the transgenic plants overexpressing *PIF5* (Fig. 6i,j), indicating that plants utilize the phyB-PIFs-mediated light signalling pathway to regulate plant growth under high salinity.

Discussion

Phosphorylation modification plays a major role in the regulation of the thermal reversion (also called dark reversion) of phyB[12,13], but the kinase(s) that phosphorylate(s) phyB has not been reported previously. Identification of such kinase(s) is critical for understanding the biological significance of the phosphorylation-mediated turnover of phyB. In this study, we discovered that FER directly interacts with and phosphorylates phyB, which is presumably the first report of a kinase

https://doi.org/10.1038/s41477-023-01390-4

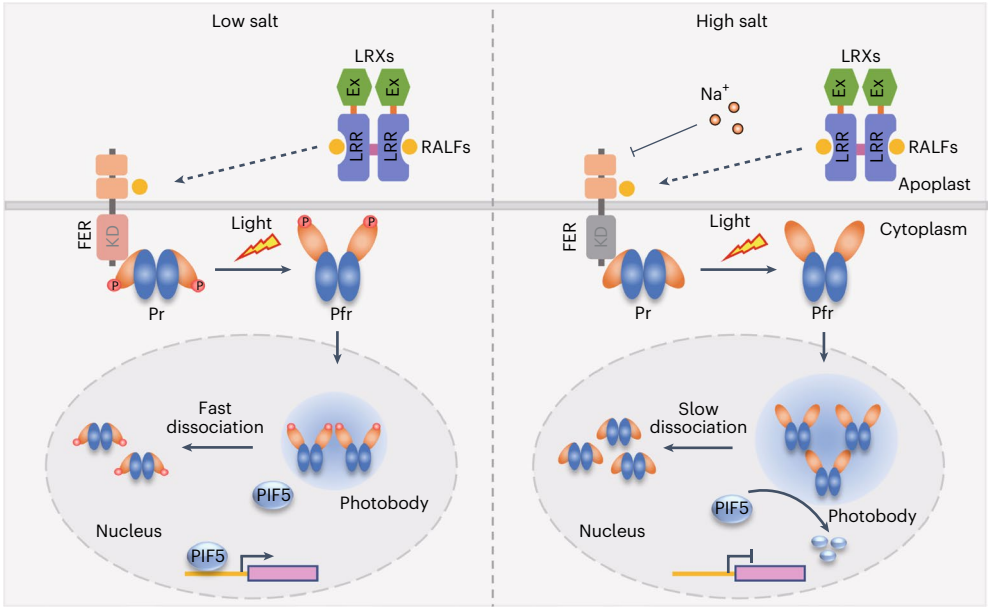

Fig. 7 | A proposed working model. Without salt stress, FER-mediated phosphorylation of phyB facilitates photobody dissociation and decreases phyB protein abundance in the nucleus, thus promoting plant growth. Under salt stress, inhibition of FER kinase activity results in the accumulation of more non-phosphorylated phyB, thus enhancing photobody stability and increasing phyB protein abundance in the nucleus, which in turn promotes PIFs degradation. As a consequence, plant growth is impaired, accompanied by the activation of the stress response. We propose that dynamic regulation of phyB accumulation in the nucleus is beneficial for plants to balance growth and stress response; however, in the *fer-4* mutant, overaccumulation of phyB in the nucleus probably leads to overactivation of the stress response, which is detrimental to the survival of plants under high salinity.

that phosphorylates phyB. Our data further support the idea that the FER-mediated phosphorylation of phyB controls photobody dynamics, which in turn regulates plant growth and salt tolerance. Collectively, this study not only identifies a kinase (FER) that phosphorylates phyB but also reveals a novel mechanism by which plants coordinate growth and salt tolerance via the FER-phyB module (Fig. 7).

The roles of the phyB-PIF module in the regulation of plant growth under salt stress have been reported in previous studies[33–35]. Under salt stress, tomato plants grown under conditions with a low R:FR ratio display higher plant height and biomass than those grown under a high R:FR ratio[33]. Overexpression of *PIF-LIKE14* (*OsPIL14*) in rice (*Oryza sativa*) promotes mesocotyl and root growth under high salinity by directly regulating cell elongation-related genes[34]. However, the early signalling components that link salt stress to phyB-PIFs-mediated growth regulation were not known. Our data showed that salt stress delays photobody dissociation via the inhibition of FER-mediated phosphorylation of phyB, and the *phyB-9* mutant or the plants overexpressing *PIF5* display longer hypocotyls under high salinity, suggesting that plants utilize the FER-phyB-PIF module to regulate growth under salt stress. FER is considered as a sensor of cell wall integrity and the cell wall status largely determines plant growth and development[36,37], hence we propose that FER may function in translating cell wall signals to regulate the phyB-mediated signalling pathway and thus dynamically fine-tunes plant growth in response to environmental stress. However, whether phyB regulates cell wall repair under salt stress requires further investigation.

The present study also showed that *phyB* mutation or overexpression of *PIF5* suppresses the leaf bleaching phenotype of both *lrx345* and *fer-4* mutants under salt stress, which further corroborates that FER and LRX3/4/5 function in a similar pathway to regulate salt tolerance. Ours and previous studies both showed that *OsphyB* mutation in rice results in an increased survival rate under salt stress[38], indicating that the phyB-mediated signalling pathway negatively regulates plant survival under salt stress. In tobacco, mutations of *phyA* and *phyB* result in an increased survival rate under salt stress, which is largely due to increased activation of antioxidant enzymes and subsequently reduced ROS accumulation[39], suggesting that the phytochromes-mediated pathways repress the accumulation of ROS under salt stress. Our recent study has shown that the enhanced leaf bleaching of the *fer-4* mutant under salt stress is caused by the overaccumulation of ROS and excessive expression of stress-responsive genes[27]. Here, gene expression analysis showed that the increased expression of salt stress- and ROS-responsive genes in the *fer-4* mutant is compromised by the *phyB-9* mutation, indicating that the suppression of salt-induced cell death of the *fer-4* mutant by the *phyB-9* mutation is to some extent attributed to attenuated stress response and ROS accumulation.

FER is a plasma membrane-localized receptor-like kinase and there has been no indication of a nuclear localization of FER, hence it is likely that the phosphorylation of phyB by FER occurs in the cytosol and then the phosphorylated phyB is transported into the nucleus to promote phyB turnover. This hypothesis is supported by our data showing that FER and phyB are co-localized in the cytosol rather than in the nucleus, and FER predominantly interacts with the Pr form of phyB. FER phosphorylates Ser106 and Ser227, and substitutions of these two phosphosites to Ala result in delayed photobody dissociation, implying that FER-mediated phosphorylation is required for the regulation of phyB thermal reversion. Apart from Ser106 and Ser227, Ser86 and Tyr104 are also phosphorylation sites that are required for modulating phyB thermal reversion[12,13], but the kinases that phosphorylate these two sites remain to be determined. Because phosphorylation of different sites at the N terminus causes a similar effect on the thermal reversion of phyB, it is possible that multiple kinases are involved in phosphorylating phyB, and this strategy enables plants to regulate phyB turnover in response to diverse developmental and environmental cues. Strikingly, in vitro analysis showed that phosphorylation of phyB by FER alone is sufficient to accelerate Pfr-to-Pr conversion, supporting the key role of phosphorylation events in the regulation of phyB turnover. Formation of photobodies is considered as an event of liquid-liquid phase separation (LLPS)[40–42], hence whether phosphorylation affects the LLPS of phyB merits further investigation.

Under salt stress, photobody dissociation is inhibited, largely due to the reduced kinase activity of FER. However, the molecular mechanisms underlying the inhibition of FER kinase activity under salt stress is still elusive. Salt stress causes modification of pectin[29,36], and recent studies showed that FER directly binds to pectin and the status of pectin is an important factor that determines FER kinase activity[29]; hence, it is possible that salt stress affects the kinase activity of FER via modification of pectin. Moreover, it has been widely demonstrated that RALFs are the ligands of FER[23,43], and our previous study showed that salt treatment induces the production of mature RALF peptides[26]. Therefore, it is likely that RALFs are required for salt-triggered inhibition of FER kinase activity. Currently, the influence of RALFs on the activation of FER remains controversial. The positive role of RALFs in the activation of FER is supported by data showing that application of synthesized mRALF1 triggers the phosphorylation of FER within 5 min[44,45]. However, the phosphorylation sites of FER induced by mRALF1, including Ser858, Ser871 and Ser877, are all located in the region after the kinase domain[44], and experimental evidence has shown that phosphorylation of Ser871 negatively regulates the kinase activity of FER[46]. Thus, we cannot rule out the possibility that RALF1-triggered phosphorylation may have a negative impact on the kinase activity of FER. Actually, the negative regulation of FER by RALFs is supported by several genetic studies showing that plants overexpressing *RALFs* or being treated with exogenous mature RALFs mimic the phenotypes of the *fer-4* mutant. For example, *fer-4* mutation and overexpression of *RALF23* both result in reduced flg22- or elf18-induced ROS bursts, enhanced stability of MYC2 and increased sensitivity to bacteria[23,47]. In addition, *fer-4* mutation and overexpression of *RALF22* both lead to a dwarf phenotype and leaf bleaching under salt stress[26,48,49]. In the future, the regulation of FER kinase activity by RALFs needs to be investigated in more detail, especially in the contexts of different developmental stages and different environmental stimuli.

Our study reveals a cross-talk between the light and salt stress signalling pathways via the FER-mediated phosphorylation of phyB, which advances our understanding of how plants rapidly and dynamically coordinate growth and stress responses under adverse environmental conditions. Our study also provides an example of how a plasma membrane-localized receptor-like kinase controls nuclear output by regulating the turnover of a nucleus-localized protein simply via a phosphorylation signature, which could be a common mechanism applicable to other receptor-like kinases. Moreover, phosphorylation-mediated regulation in response to environmental conditions may also be applied to other photoreceptors, such as other phytochromes and cryptochromes, all of which have been reported to undergo phosphorylation modifications[50–52]. Remarkably, *phyB* mutation or overexpression of *PIF* genes not only promotes plant growth but also largely enhances plant survival under salt stress, which provides important genetic loci for the engineering of salt-tolerant crops without growth penalty.

Methods

Plant materials and growth conditions

The Columbia (Col-0) or Landsberg erecta (Ler) ecotype of *A. thaliana* and the Nipponbare of rice (*Oryza sativa*) were used as the wild-type plant materials. *lrx345*, *fer-4* and *proFER::FER-GFP* transgenic plants have been described previously[26]. *phyB-9* (CS6217), *pif5-3* (SALK_087012) and *pifq* (CS66049) mutants were obtained from the *Arabidopsis* Biological Resource Center (ABRC). The $phyB^{Y276H}$/*phyB-5* (YHB, in Ler background) was obtained from Prof. J. Clark Lagarias (University of California, Davis, USA). Transgenic plants expressing *p35S::phyB*^{WT}*-GFP*, *p35S::phyB*^{S106AS227A}*-GFP*, *p35S::phyB*^{S106DS227D}*-GFP*, *p35S::PIF5-YFP*, *phyBpro::phyB-Myc* and *p35S::PIF3-GFP* were generated by *Agrobacterium tumefaciens* strain GV3101-mediated transformation. *OsphyB* mutant was a gift from Prof. Rongxiang Fang (Institute of Microbiology, CAS, China). Primers used for genotyping are listed in Supplementary Table 3.

Seeds were sterilized with 15% bleach and sown on 1/2 MS medium with 0.8% agar and 1% sucrose (w/v). After stratification at 4 °C for 2 to 4 d, the plates were placed in a growth chamber at 22 °C with a long-day light cycle (LD, 16 h light/8 h dark, with light intensity of 100 μmol m^{-2} s^{-1}). Measurement of the fluence rate curve was performed as described previously[53]. The seeds were sown on 1/2 MS medium without sucrose and transferred to white light for 4 h at 22 °C to trigger germination, and then the germinated seeds were transferred to the continuous red light (LED; 660 nm) under various fluence conditions for 4 d. For survival rate measurement, plants were grown on 120 mM NaCl medium under normal white light (NL, ~100 μmol m^{-2} s^{-1}) or weak white-light (WL, ~5 μmol m^{-2} s^{-1}) conditions with a 16 h light/8 h dark light cycle, and survival rate was measured after growing for approximately 8 d. For survival rate measurement under red-light illumination, plants grown on 120 mM NaCl medium were exposed to continuous high red-light intensity (~15 μmol m^{-2} s^{-1}) or continuous low red-light intensity (~1 μmol m^{-2} s^{-1}), and survival rate was quantified after growing for approximately 8 d. Measurement of survival rate of rice under salt stress was performed as described previously[54]. Briefly, germinated seeds were transferred to Yoshida's culture solution and placed in a growth chamber at 28 °C with a short-day light cycle (SD, 8 h light/16 h dark). Two-week-old seedlings were treated with 100 mM NaCl and survival rate was calculated after growing for 12 d.

Measurement of plant size

For petiole length measurement, 7-day-old seedlings were transferred to soil and grown for 22 d. The largest expanded rosette leaf was excised from each plant and the length of petiole was measured. For hypocotyl measurement, plants were grown in growth chambers at 22 °C under LD conditions for 4 d, and the plants were then grown in darkness for 3 d. For hypocotyl measurement under salt stress, seedlings were grown in a growth chamber at 22 °C under LD conditions for 3 d and then transferred to 1/2 MS medium supplemented with NaCl. The seedlings were grown under dark conditions for an additional 5 d before hypocotyl length measurement using ImageJ software. For plant height measurement, 7-day-old seedlings were transferred to soil. After growth under LD light conditions for 28 d, plant height was measured.

Plasmid construction

For the generation of transgenic plants, the coding sequence (CDS) of *phyB* was amplified and cloned into pEarleyGate 103 vector using the XhoI restriction site. pEarleyGate 103-phyB^{S106AS227A} and pEarleyGate 103-phyB^{S106DS227D} constructs were generated by PCR-based point mutation using PrimerSTAR Max DNA polymerase (Takara). To generate pEarleyGate101-PIF5, the CDS of *PIF5* was amplified and cloned into pDONR207 using a BP Clonase II kit (Thermo Fisher), and then pDONR207-PIF5 was recombined into pEarleyGate101 using an LR Clonase II kit (Thermo Fisher). To generate pCambia1300 PIF3-GFP, the CDS of *PIF3* was amplified and cloned into pCambia1300-GFP using the BamHI and SalI restriction sites. For yeast two-hybrid assay, the CDS of *phyB*, *phyBN* (1–651 amino acid (aa)) and *phyBC* (652-1172 aa) were amplified and cloned into pGADT7 using the EcoRI and BamHI restriction sites. The CDS sequence of *FERKD* (536–895 aa) was amplified and cloned into pGBKT7 using the EcoRI and BamHI restriction sites. For split luciferase complementation assay, the CDS of *phyB*, *phyBN*, *phyBC*, *FER*, *FERCD* (470–895 aa) and THE1 were amplified and cloned into pDONR207 before being recombined into nLUC or cLUC vector. For recombinant protein expression, the CDS of *FERCD* was amplified and cloned into pET28a using the EcoRI and SalI restriction sites. The pET28a-FERCD^{K565R} construct was generated by PCR-based point mutation. The phyBN^{S106AS227A}, phyBN^{S86A} and phyBN^{S86AS106AS227A} constructs for the expression of recombinant proteins were generated by PCR-based point mutation using phyBN plasmid (PMH1105, Addgene) as a template. All primers used for plasmid construction are listed in Supplementary Table 3.

Mutant screening and BSA

The *lrx345* mutant seeds were mutagenized with ethylmethane sulfonate, and suppressors were screened in the M_2 generation. The identified suppressor *slrx620* was crossed with *lrx345*. In the F_2 population, approximately 120 plants that survived on NaCl medium were pooled for genomic DNA extraction using a DNeasy Plant Maxi kit (QIAGEN). The isolated DNA was sent for Illumina sequencing and BSA was performed according to a protocol described previously[55].

RNA extraction and RT–qPCR

Seeds were sterilized and sown on 1/2 MS medium with 0.8% agar and 1% sucrose (w/v). After stratification at 4 °C for 2 d, the plates were placed in a growth chamber under white light in LD conditions at 22 °C for 8 d. Total RNAs were extracted from whole seedlings using an Eastep Total RNA Super Extraction kit (Promega) according to the manufacturer's instructions. Complementary DNA (cDNA) was synthesized from messenger RNA (mRNA) using ABScript III RT Master Mix for qPCR with gDNA Remover kit (ABclonal). Quantitative PCR with reverse transcription (RT–qPCR) was performed using i*Taq*Universal SYBR Green Supermix (Bio-Rad). Primers used for RT–qPCR are listed in Supplementary Table 3.

Yeast two-hybrid assay

Bait vector pGBKT7 and prey vector pGBKT7 harbouring FERKD or phyB were co-transformed into yeast strain AH109. After incubation at 30 °C for 2 d, positive yeast colonies containing bait and prey constructs were selected on SD/-Trp/-Leu plates. The selected yeast colonies were incubated in liquid medium overnight at 30 °C, and then the yeast cells were diluted to an optical density $(OD)_{600}$ of 0.5 and spotted on SD/-Trp/-Leu or SD/-Trp/-Leu/-His medium.

Split luciferase complementation assay

A split luciferase complementation assay was performed using *N. benthamiana* leaves. nLUC or cLUC fused with the tested genes was introduced into *A. tumefaciens* strain GV3101. Strain colonies were incubated in LB liquid medium overnight, and bacterial cells were resuspended in infiltration buffer (10 mM $MgCl_2$, 10 mM MES (pH 5.7) and 200 μM acetosyringone) and diluted to an OD_{600} of 0.5. After incubation at room temperature for 3 h in the dark, cell suspensions were injected into *N. benthamiana*. After 48 h, luciferin was sprayed on tobacco leaves and fluorescence was detected using plant living imaging system NightShade LB985.

Recombinant protein expression and in vitro kinase assay

Recombinant phyB-Avi-His encoded by the plasmid pMH1105 was purified as previously described[31]. The construct of PMH1105-phyBN, PMH1105-phyBN^{S86A}, PMH1105-phyBN^{S106AS227A} or PMH1105-phyBN^{S86AS106AS227A} was transformed into strain BL21 Star (DE3) (WEDI). The bacteria were incubated in LB liquid medium at 37 °C until OD_{600} reached 0.8, and then isopropyl b-D-1-thiogalactopyranoside (IPTG, 1 mM final concentration) was added to the cell culture and incubated at 16 °C for 18 h. Bacterial solutions were centrifuged and pellets were resuspended in lysis buffer (50 mM HEPES, 300 mM NaCl, 20 mM imidazole, 5% (v/v) glycerol and 1 mM tris(2-carboxyethyl)phosphine (TCEP) at pH 7.5) and lysed using a high-pressure homogenizer. The samples were loaded into a Histrap HP column (Cytiva) and eluted with an imidazole linear gradient of 20–500 mM imidazole using an Äkta system at 4 °C. The proteins were concentrated and loaded into a Superdex 200 column (Cytiva) pre-equilibrated with protein buffer (1x PBS and 0.5 mM TCEP). For recombinant His-FERCD purification, pET28a-FERCD or pET28a-FERCD^{K565R} construct was transformed into strain BL21-CodonPlus (DE3)-RIPL (WEDI). After overnight induction at 16 °C with 1 mM IPTG, the bacterial solution was centrifuged and pellet was resuspended in lysis buffer (20 mM HEPES, 300 mM NaCl, 20 mM imidazole, 1% (v/v) Triton X-100 and 1 mM TCEP at pH 7.5) and lysed using a high-pressure homogenizer. The sample was loaded into a Histrap HP column and eluted with an imidazole linear gradient of 20–500 mM imidazole using an Äkta system at 4 °C. Then, the recombinant protein was purified with a Hitrap Q FF column (Cytiva) using a 20–500-mM linear NaCl gradient.

An in vitro kinase assay was performed using ATP-gamma-S (Abcam) as previously described[56]. phyBN^{WT}, phyBN^{S86A} or phyBN-^{S106AS227A} was incubated with His-FERCD in 25 μl kinase buffer (50 mM HEPES (pH 7.5), 5 mM $MgCl_2$, 1 mM dithiothreitol (DTT) and 1 mM ATP-gamma-S). The mixture was incubated at room temperature for 30 min before the proteins were mixed with 2.5 mM *p*-Nitrobenzyl mesylate (Abcam) and incubated at room temperature for 2 h. After adding 1x SDS loading buffer, the phosphorylated proteins were detected by immunoblotting using anti-thiophosphate ester antibody (Abcam, ab92570) and total protein inputs were visualized by Coomassie brilliant blue (CBB) staining.

Protein extraction and Co-IP assay

Proteins were extracted using lysis buffer (50 mM Tris-HCl (pH 7.5), 150 mM NaCl, 0.5 mM EDTA, 5% (v/v) glycerol, 1 mM DTT, 1 mM phenylmethylsulfonyl fluoride (PMSF), 1x complete protease inhibitor cocktail and 0.1% (v/v) NP-40). The extraction buffer was centrifuged at 14,000 × *g* and 4 °C for 10 min and the supernatant was transferred to a new 1.5 ml Eppendorf tube. The total protein concentration of each sample was measured and adjusted to the same level using Quick Start Bradford Dye reagent (Bio-Rad). The protein samples were boiled with 1x SDS loading buffer and analysed by immunoblotting. The proteins were detected by using anti-GFP (Sigma, 11814460001, 1:3,000 dilution), anti-phyB (phytoAB, PHY1733, 1:2,000 dilution) or anti-PIF5 (Agrisera, AS12 2112, 1:1,000 dilution) antibodies, and goat anti-mouse HRP conjugate (Bio-Rad, 1721011, 1:10,000 dilution) or goat anti-rabbit HRP conjugate (Bio-Rad, 1721019, 1:10,000 dilution) was used as a secondary antibody.

For Co-IP assay in dark or red-light conditions, *FERpro::FER-GFP* and *FERpro::FER-GFP/phyBpro::phyB-Myc* seedlings were grown under dark conditions for 7 d and then transferred to red light or kept under darkness for 6 h. Total proteins were extracted from whole seedlings using the same lysis buffer described above. After centrifugation, the supernatant was incubated at 4 °C for 4 h with anti-Myc antibody (Cell Signaling Technology, 2278) and then incubated with protein G agarose (Millipore, 16-266) for 2 h at 4 °C. The beads were washed twice with wash buffer (50 mM Tris-HCl (pH 7.5), 150 mM NaCl and 0.5 mM EDTA) and once with 1x PBS. After centrifugation, the beads were boiled with 2x SDS sample buffer for 10 min. The immunoprecipitated proteins were detected by SDS–PAGE using anti-Myc and anti-GFP antibodies.

In vivo phosphorylation assay

For phosphorylation assay in vivo, seedlings were grown on 1/2 MS or 100 mM NaCl medium (without sucrose) in the dark for 7 d. Total proteins were extracted using lysis buffer (50 mM Tris-HCl (pH 7.5), 150 mM NaCl, 1% (v/v) Triton X-100, 1 mM PMSF, 1x complete protease inhibitor cocktail and 1x phosphatase inhibitor cocktail set II (Millipore, 524625)). The extraction buffer was centrifuged twice at 14,000 × *g* at 4 °C for 10 min, and the supernatant was transferred to a new tube. The total protein concentration of each sample was measured and adjusted to the same level using Quick Start Bradford Dye reagent. Then, the protein extract was incubated with anti-GFP magarose beads (Smart-lifesciences, SM038001) for 4 h at 4 °C. The beads were washed four times in washing buffer (50 mM Tris-HCl (pH 7.5), 150 mM NaCl, 0.1% (v/v) Triton X-100) and twice with 1x PBS. The beads were boiled with 2x SDS sample buffer for 10 min and the immunoprecipitated proteins were detected by SDS–PAGE using anti-phosphoserine (Abcam, ab9332, 1:125 dilution) and anti-GFP antibodies.

For mass spectrometry analysis in vivo, the beads containing immunoprecipitated phyB-GFP were dissolved in lysis buffer with

guanidine hydrochloride, TCEP and calcium acetylacetonate and incubated at 65 °C for 5 min. After centrifugation at 14,000 *g* for 15 min, ammonium bicarbonate and trypsin (1:50) were added to each sample and the sample incubated overnight at 37 °C. After digestion, chromatographic separation was performed using an Easy nLC 1200 chromatographic system (Thermo Fisher). Then, the peptides were analysed with the targeted parallel reaction monitoring method using a Q Exactive HF-X mass spectrometer (Thermo Fisher). Peak lists were generated using Proteome Discoverer. For quantitative analysis, the phosphopeptide signal was calculated from the peak areas of the non-phosphorylated and the phosphorylated peptides according to the following equation: Phosphopeptide signal = Phosphopeptide peak area / (Phosphopeptide peak area+ non-phosphorylated peptide peak area).

Nuclear fractionation

For nuclear fractionation assay, seedlings were grown under LD conditions for 6 d and then transferred to the dark for 3 d. For salt stress treatment, 6-day-old seedlings were transferred into 1/2 liquid MS with or without 120 mM NaCl and then placed in the dark for 3 d. Nuclear fractionation assay was performed as described previously[57]. Total proteins were extracted from seedlings using fractionation extraction buffer (2.5% (w/w) Ficoll 400, 5% (w/w) dextran T40, 0.4 M sucrose, 25 mM Tris-HCl (pH 7.5), 10 mM $MgCl_2$, 1 mM DTT, 1 mM PMSF and 1x complete protease inhibitor cocktail). The mixture was filtered twice with one layer of Miracloth (Millipore) and the homogenate with the same concentration was used as total protein. For nuclear protein extraction, the homogenate was incubated with 0.5% (v/v) Triton X-100 on ice for 15 min and centrifuged at 1,500 *g* for 5 min at 4 °C. The supernatant was used as cytosolic proteins. The pellet was washed twice with wash buffer (2.5% (w/w) Ficoll 400, 5% (w/w) dextran T40, 0.4 M sucrose, 25 mM Tris-HCl (pH 7.5), 10 mM $MgCl_2$ and 0.1% (v/v) Triton X-100), resuspended in 80 µl of fractionation extraction buffer, and the suspension was used as nuclear protein. Immunoblottings were performed using anti-phyB, anti-PEPC (Agrisera, AS09458, 1:2,000 dilution) and anti-H3 (Millipore, 07-690, 1:10,000 dilution) antibodies. Band abundance was estimated using ImageJ. In each fractionation, wild-type sample at 0 h was set as 1 and the band abundance of other samples was divided by the value of the wild-type sample at 0 h.

Analysis of the kinase activity of FER

Seven-day-old *proFER::FER-GFP* seedlings grown under LD conditions were transferred into 1/2 liquid MS for 12 h and then treated with H_2O or 150 mM NaCl for 5 min. Total proteins were extracted from these seedlings using protein lysis buffer. After centrifugation, the supernatant was incubated at 4 °C for 4 h with anti-GFP magarose beads. Then, the beads were washed twice with wash buffer (50 mM Tris-HCl (pH 7.5), 150 mM NaCl and 0.5 mM EDTA), twice with 1x PBS and twice with kinase buffer (50 mM HEPES (pH 7.5) and 1 mM DTT). The pellet was resuspended in 10 µl kinase buffer. The immunoprecipitated proteins were incubated in 25 µl kinase buffer (50 mM HEPES (pH 7.5), 5 mM $MgCl_2$, 1 mM DTT and 1 mM ATP-gamma-S) for 30 min at room temperature. Then, the reaction buffer was mixed with 2.5 mM *p*-Nitrobenzyl mesylate and incubated at room temperature for 2 h. Autophosphorylation of FER was detected by immunoblotting using an anti-thiophosphate ester antibody.

Confocal imaging

Confocal microscopy was performed with a Leica TCS SMD FLCS confocal laser scanning microscope. Green fluorescent protein (GFP) was excited at 488 nm using argon and collected with a 510–550 nm detector. mCherry was excited at 561 nm using argon and collected with a 610–650 nm detector. For light to dark treatment, seedlings were grown on 1/2 MS under LD conditions for 5 d and then the seedlings were exposed to light for 5 h before being subjected to dark treatment for 1 h and 3 h. For salt treatment, after growth on 1/2 MS under LD conditions for 5 d, the seedlings were transferred to 1/2 MS medium supplemented with NaCl at ZT0. After 5 h of light exposure, the seedlings were kept in the dark for 1 h and 3 h before observation of photobodies.

Pfr-to-Pr conversion analysis

In vitro Pfr-to-Pr conversion analysis of recombinant phyB protein was performed as previously described[31]. For the assessment of Pfr-to-Pr conversion after red or far-red light illumination, the recombinant phyBN proteins together with chromophore phycocyanobilin (PCB) were incubated in a protein buffer (1x PBS and 0.5 mM TCEP) and illuminated for 5 min with 660 (~17 µmol m^{-2} s^{-1}) or 740 nm (~5 µmol m^{-2} s^{-1}) light before measurement. For the measurement of Pfr-to-Pr conversion after dark treatment, $phyBN^{WT}$ and the mutated variants of phyBN were illuminated with 660 nm (~17 µmol m^{-2} s^{-1}) light for 5 min and then placed under dark conditions. To test the influence of FER on Pfr-to-Pr conversion, $phyBN^{WT}$ alone or $phyB^{WT}$ incubated with His-FERCD or His-$FERCD^{K565R}$ in kinase buffer (50 mM HEPES (pH 7.5), 5 mM $MgCl_2$, 1 mM DTT and 1 mM ATP) was illuminated at 660 nm (~17 µmol m^{-2} s^{-1}) for 5 min and then subjected to dark treatment. Absorption spectra at 651 nm (Pr form) and 714 nm (Pfr form) were measured using a Nanodrop 2000C spectrophotometer and the Pfr/Pr ratio was calculated. All experiments were performed at the same temperature.

RNA-seq analysis

Total RNAs were extracted from 8-day-old seedlings using an RNeasy Plant Mini kit (Qiagen) according to the manufacturer's instructions. Three biological replicates were performed for each genotype. Reads of RNA-seq data were mapped to the *Arabidopsis* reference genome (TAIR10) using HISAT2. Differentially expressed genes between the samples were identified using the R package edgeR (FDR < 0.05, FC > 1.5). Venn diagrams were created using Venny (https://bioinfogp.cnb.csic.es/tools/ venny/index.html). GO enrichment analysis was performed using AgriGO[58] (http://systemsbiology.cau.edu.cn/agriGOv2/index.php).

Quantification and statistical analysis

Quantification and statistical parameters are indicated in the legends of each figure. Statistical analyses were carried out using Student's *t*-test (two-sided) for two groups or one-way analysis of variance (ANOVA) followed by Duncan analysis for multiple groups. A *P* value less than 0.05 was considered significant. All graphs were generated using GraphPad Prism v8 for windows or Microsoft Excel for windows.

Reporting summary

Further information on research design is available in the Nature Portfolio Reporting Summary linked to this article.

Data availability

All materials in this study are available from the corresponding author upon request. The raw data of BSA sequencing have been deposited in the NCBI BioProject database under accession number PRJNA914087. RNA-seq data have been deposited in the NCBI GEO under accession number GSE188335. *Arabidopsis* reference genome (TAIR10) was used in this study. Source data are provided with this paper.

References

1. Kami, C., Lorrain, S., Hornitschek, P. & Fankhauser, C. Light-regulated plant growth and development. *Curr. Top. Dev. Biol.* **91**, 29–66 (2010).
2. Nagy, F. & Schafer, E. Phytochromes control photomorphogenesis by differentially regulated, interacting signaling pathways in higher plants. *Annu. Rev. Plant Biol.* **53**, 329–355 (2002).
3. Rockwell, N. C., Su, Y. S. & Lagarias, J. C. Phytochrome structure and signaling mechanisms. *Annu. Rev. Plant Biol.* **57**, 837–858 (2006).

4. Al-Sady, B., Ni, W., Kircher, S., Schafer, E. & Quail, P. H. Photoactivated phytochrome induces rapid PIF3 phosphorylation prior to proteasome-mediated degradation. *Mol. Cell* **23**, 439–446 (2006).
5. Yamaguchi, R., Nakamura, M., Mochizuki, N., Kay, S. A. & Nagatani, A. Light-dependent translocation of a phytochrome B-GFP fusion protein to the nucleus in transgenic *Arabidopsis*. *J. Cell Biol.* **145**, 437–445 (1999).
6. Bae, G. & Choi, G. Decoding of light signals by plant phytochromes and their interacting proteins. *Annu. Rev. Plant Biol.* **59**, 281–311 (2008).
7. Huang, H. et al. PCH1 regulates light, temperature, and circadian signaling as a structural component of phytochrome B-photobodies in *Arabidopsis*. *Proc. Natl Acad. Sci. USA* **116**, 8603–8608 (2019).
8. Sweere, U. et al. Interaction of the response regulator ARR4 with phytochrome B in modulating red light signaling. *Science* **294**, 1108–1111 (2001).
9. Mira-Rodado, V. et al. Functional cross-talk between two-component and phytochrome B signal transduction in *Arabidopsis*. *J. Exp. Bot.* **58**, 2595–2607 (2007).
10. Galvao, R. M. et al. Photoactivated phytochromes interact with HEMERA and promote its accumulation to establish photomorphogenesis in *Arabidopsis*. *Genes Dev.* **26**, 1851–1863 (2012).
11. Chen, M. et al. *Arabidopsis* HEMERA/pTAC12 initiates photomorphogenesis by phytochromes. *Cell* **141**, 1230–1240 (2010).
12. Medzihradszky, M. et al. Phosphorylation of phytochrome B inhibits light-induced signaling via accelerated dark reversion in *Arabidopsis*. *Plant Cell* **25**, 535–544 (2013).
13. Nito, K., Wong, C. C., Yates, J. R. 3rd & Chory, J. Tyrosine phosphorylation regulates the activity of phytochrome photoreceptors. *Cell Rep.* **3**, 1970–1979 (2013).
14. Reed, J. W., Nagpal, P., Poole, D. S., Furuya, M. & Chory, J. Mutations in the gene for the red/far-red light receptor phytochrome B alter cell elongation and physiological responses throughout *Arabidopsis* development. *Plant Cell* **5**, 147–157 (1993).
15. Jung, J.-H. et al. Phytochromes function as thermosensors in Arabidopsis. *Science* **354**, 886–889 (2016).
16. Legris, M. et al. Phytochrome B integrates light and temperature signals in *Arabidopsis*. *Science* **354**, 897–900 (2016).
17. Campos, M. L. et al. Rewiring of jasmonate and phytochrome B signalling uncouples plant growth-defense tradeoffs. *Nat. Commun.* **7**, 12570 (2016).
18. Zhao, C., Zhang, H., Song, C., Zhu, J. K. & Shabala, S. Mechanisms of plant responses and adaptation to soil salinity. *Innovation* **1**, 100017 (2020).
19. Franck, C. M., Westermann, J. & Boisson-Dernier, A. Plant malectin-like receptor kinases: from cell wall integrity to immunity and beyond. *Annu. Rev. Plant Biol.* **69**, 301–328 (2018).
20. Duan, Q. et al. FERONIA controls pectin- and nitric oxide-mediated male-female interaction. *Nature* **579**, 561–566 (2020).
21. Escobar-Restrepo, J. M. et al. The FERONIA receptor-like kinase mediates male-female interactions during pollen tube reception. *Science* **317**, 656–660 (2007).
22. Li, C. et al. Glycosylphosphatidylinositol-anchored proteins as chaperones and co-receptors for FERONIA receptor kinase signaling in *Arabidopsis*. *eLife* **4**, e06587 (2015).
23. Stegmann, M. et al. The receptor kinase FER is a RALF-regulated scaffold controlling plant immune signaling. *Science* **355**, 287–289 (2017).
24. Zhu, S. et al. The RALF1-FERONIA complex phosphorylates eIF4E1 to promote protein synthesis and polar root hair growth. *Mol. Plant* **13**, 698–716 (2020).
25. Liao, H., Tang, R., Zhang, X., Luan, S. & Yu, F. FERONIA receptor kinase at the crossroads of hormone signaling and stress responses. *Plant Cell Physiol.* **58**, 1143–1150 (2017).
26. Zhao, C. et al. Leucine-rich repeat extensin proteins regulate plant salt tolerance in *Arabidopsis*. *Proc. Natl Acad. Sci. USA* **115**, 13123–13128 (2018).
27. Zhao, C. et al. The LRXs-RALFs-FER module controls plant growth and salt stress responses by modulating multiple plant hormones. *Natl Sci. Rev.* **8**, nwaa149 (2021).
28. Huq, E., Al-Sady, B. & Quail, P. H. Nuclear translocation of the photoreceptor phytochrome B is necessary for its biological function in seedling photomorphogenesis. *Plant J.* **35**, 660–664 (2003).
29. Gigli-Bisceglia, N., van Zelm, E., Huo, W., Lamers, J. & Testerink, C. *Arabidopsis* root responses to salinity depend on pectin modification and cell wall sensing. *Development* **149**, dev200363 (2022).
30. Wagner, D., Tepperman, J. M. & Quail, P. H. Overexpression of phytochrome B induces a short hypocotyl phenotype in transgenic *Arabidopsis*. *Plant Cell* **3**, 1275–1288 (1991).
31. Horner, M., Yousefi, O. S., Schamel, W. W. A. & Weber, W. Production, purification and characterization of recombinant biotinylated phytochrome B for extracellular optogenetics. *Bio Protoc.* **10**, e3541 (2020).
32. Su, Y. S. & Lagarias, J. C. Light-independent phytochrome signaling mediated by dominant GAF domain tyrosine mutants of *Arabidopsis* phytochromes in transgenic plants. *Plant Cell* **19**, 2124–2139 (2007).
33. Wang, Y., Bian, Z., Pan, T., Cao, K. & Zou, Z. Improvement of tomato salt tolerance by the regulation of photosynthetic performance and antioxidant enzyme capacity under a low red to far-red light ratio. *Plant Physiol. Biochem.* **167**, 806–815 (2021).
34. Mo, W. et al. PHYTOCHROME-INTERACTING FACTOR-LIKE14 and SLENDER RICE1 interaction controls seedling growth under salt stress. *Plant Physiol.* **184**, 506–517 (2020).
35. Junior, C. A. S., D'Amico-Damião, V. & Carvalho, R. F. Phytochrome type B family: the abiotic stress responses signaller in plants. *Ann. Appl. Biol.* **178**, 135–148 (2020).
36. Feng, W. et al. The FERONIA receptor kinase maintains cell-wall integrity during salt stress through Ca^{2+} signaling. *Curr. Biol.* **28**, 666–675.e5 (2018).
37. Vaahtera, L., Schulz, J. & Hamann, T. Cell wall integrity maintenance during plant development and interaction with the environment. *Nat. Plants* **5**, 924–932 (2019).
38. Kwon, C. T. et al. Functional deficiency of phytochrome B improves salt tolerance in rice. *Environ. Exp. Bot.* **148**, 100–108 (2018).
39. Yang, T., Lv, R., Li, J., Lin, H. & Xi, D. Phytochrome A and B negatively regulate salt stress tolerance of *Nicotiana tobacum* via ABA-jasmonic acid synergistic cross-talk. *Plant Cell Physiol.* **59**, 2381–2393 (2018).
40. Banani, S. F., Lee, H. O., Hyman, A. A. & Rosen, M. K. Biomolecular condensates: organizers of cellular biochemistry. *Nat. Rev. Mol. Cell Biol.* **18**, 285–298 (2017).
41. Wang, X. et al. A photoregulatory mechanism of the circadian clock in *Arabidopsis*. *Nat. Plants* **7**, 1397–1408 (2021).
42. Chen, D. et al. Integration of light and temperature sensing by liquid-liquid phase separation of phytochrome B. *Mol. Cell* **82**, 3015–3029.e6 (2022).
43. Xiao, Y. et al. Mechanisms of RALF peptide perception by a heterotypic receptor complex. *Nature* **572**, 270–274 (2019).
44. Haruta, M., Sabat, G., Stecker, K., Minkoff, B. B. & Sussman, M. R. A peptide hormone and its receptor protein kinase regulate plant cell expansion. *Science* **343**, 408–411 (2014).

45. Chen, J. et al. FERONIA interacts with ABI2-type phosphatases to facilitate signaling cross-talk between abscisic acid and RALF peptide in *Arabidopsis*. *Proc. Natl Acad. Sci. USA* **113**, E5519–E5527 (2016).
46. Minkoff, B. B. et al. A cell-free method for expressing and reconstituting membrane proteins enables functional characterization of the plant receptor-like protein kinase FERONIA. *J. Biol. Chem.* **292**, 5932–5942 (2017).
47. Guo, H. et al. FERONIA receptor kinase contributes to plant immunity by suppressing jasmonic acid signaling in *Arabidopsis thaliana*. *Curr. Biol.* **28**, 3316–3324.e6 (2018).
48. Duan, Q., Kita, D., Li, C., Cheung, A. Y. & Wu, H. M. FERONIA receptor-like kinase regulates RHO GTPase signaling of root hair development. *Proc. Natl Acad. Sci. USA* **107**, 17821–17826 (2010).
49. Zhang, X., Yang, Z., Wu, D. & Yu, F. RALF-FERONIA signaling: linking plant immune response with cell growth. *Plant Commun.* **1**, 100084 (2020).
50. Kim, J. I. et al. Phytochrome phosphorylation modulates light signaling by influencing the protein-protein interaction. *Plant Cell* **16**, 2629–2640 (2004).
51. Ryu, J. S. et al. Phytochrome-specific type 5 phosphatase controls light signal flux by enhancing phytochrome stability and affinity for a signal transducer. *Cell* **120**, 395–406 (2005).
52. Shalitin, D. et al. Regulation of *Arabidopsis* cryptochrome 2 by blue-light dependent phosphorylation. *Nature* **417**, 758–763 (2002).
53. Viczian, A. et al. Differential phosphorylation of the N-terminal extension regulates phytochrome B signaling. *New Phytol.* **225**, 1635–1650 (2020).
54. Wang, J. et al. A DNA methylation reader-chaperone regulator-transcription factor complex activates OsHKT1;5 expression during salinity stress. *Plant Cell* **32**, 3535–3558 (2020).
55. Li, H. & Durbin, R. Fast and accurate short read alignment with Burrows-Wheeler transform. *Bioinformatics* **25**, 1754–1760 (2009).
56. Allen, J. J. et al. A semisynthetic epitope for kinase substrates. *Nat. Methods* **4**, 511–516 (2007).
57. Qian, C. et al. Dual-source nuclear monomers of UV-B light receptor direct photomorphogenesis in *Arabidopsis*. *Mol. Plant* **9**, 1671–1674 (2016).
58. Du, Z., Zhou, X., Ling, Y., Zhang, Z. & Su, Z. agriGO: a GO analysis toolkit for the agricultural community. *Nucleic Acids Res.* **38**, W64–W70 (2010).

Acknowledgements

We thank H. Yang (Shanghai Normal University, China) for providing *phyBpro::phyB-Myc* plasmid, R. Fang (Institute of Microbiology, CAS, China) for providing *OsphyB* mutant, and J. Clark Lagarias (University of California, Davis, USA) for providing *YHB* seeds. This work was supported by National Natural Science Foundation of China Grant No. 32070295 (to C.Z.), Shanghai Pujiang Program Grant No. 20PJ1414800 (to C.Z.), Shanghai Agriculture Applied Technology Development Program Grant No. X20200101 (to C.Z.), and Strategic Priority Research Program of the Chinese Academy of Sciences Grant No. XDA27040104 (to J.-K.Z.).

Author contributions

X.L. and C.Z. conceived and designed the experiments; X.L., W.J., Y.L., H.N., C.L., J.L. and M.L. performed experiments; X.L., L.C., L.P. and B.Z. conducted bioinformatic analysis; X.L. and R.L. performed proteomics analysis; L.T., H.W., J.Y., P.W., H.L., J.-K.Z. and C.Z. analysed data; X.L., J.-K.Z. and C.Z. wrote the paper.

Competing interests

The authors declare no competing interests.

Additional information

Extended data is available for this paper at https://doi.org/10.1038/s41477-023-01390-4.

Supplementary information The online version contains supplementary material available at https://doi.org/10.1038/s41477-023-01390-4.

Correspondence and requests for materials should be addressed to Jian-Kang Zhu or Chunzhao Zhao.

Peer review information *Nature Plants* thanks Ferenc Nagy, Eunkyoo Oh, Christa Testerink and the other, anonymous, reviewer(s) for their contribution to the peer review of this work.

https://doi.org/10.1038/s41477-023-01390-4

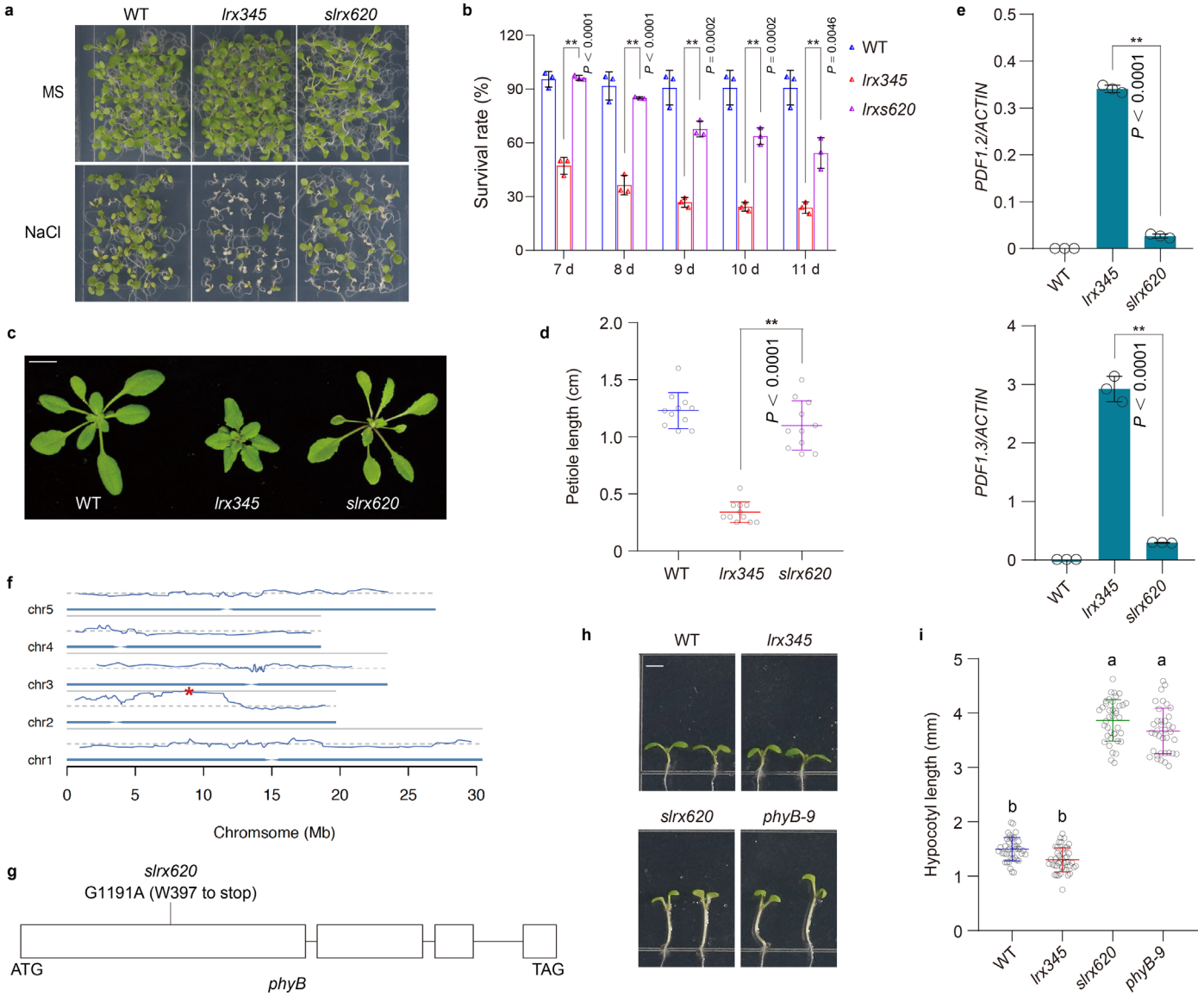

Extended Data Fig. 1 | *slrx620* mutation suppresses the phenotypes of *lrx345* mutant. a, Phenotype of wild type, *lrx345*, and *slrx620* mutant grown on 1/2 MS medium with or without NaCl (120 mM) under white light conditions (16 h light/8 h dark cycle). **b**, Quantification of the survival rate of seedlings grown on NaCl medium. Values are the means ± SD of three biological replicates. **c**, Representative images of wild type, *lrx345*, and *slrx620* mutant grown on soils for 22 days under LD conditions. Scale bar, 1 cm. **d**, Quantification of the petiole length of plants shown in **c**. Values are the means ± SD (n = 11 seedlings). **e**, RT–qPCR analysis of the transcript levels of *PDF1.2* and *PDF1.3* genes in each genotype. Values are the means ± SD of three biological replicates. **f**, Identification of mutations in *slrx620* mutant by bulked segregant analysis (BSA). Red asterisk indicates the location of the mutated gene that is associated with the *slrx620* mutant phenotypes. **g**, Diagram illustrating the genomic structure of *phyB* and the mutation site in the *slrx620* mutant. **h**. Hypocotyl growth of seedlings grown under white light conditions for 4 days. Scale bar, 2 mm. **i**, Quantification of the hypocotyl length of the seedlings shown in **h**. Values are the means ± SD (n = 49-63 seedlings). Asterisks in **b**, **d** and **e** indicate statistically significant differences ($^{**}P < 0.01$, Student's *t* test, two-sided). Different letters in **i** indicate statistically significant differences ($P < 0.01$, one-way ANOVA).

https://doi.org/10.1038/s41477-023-01390-4

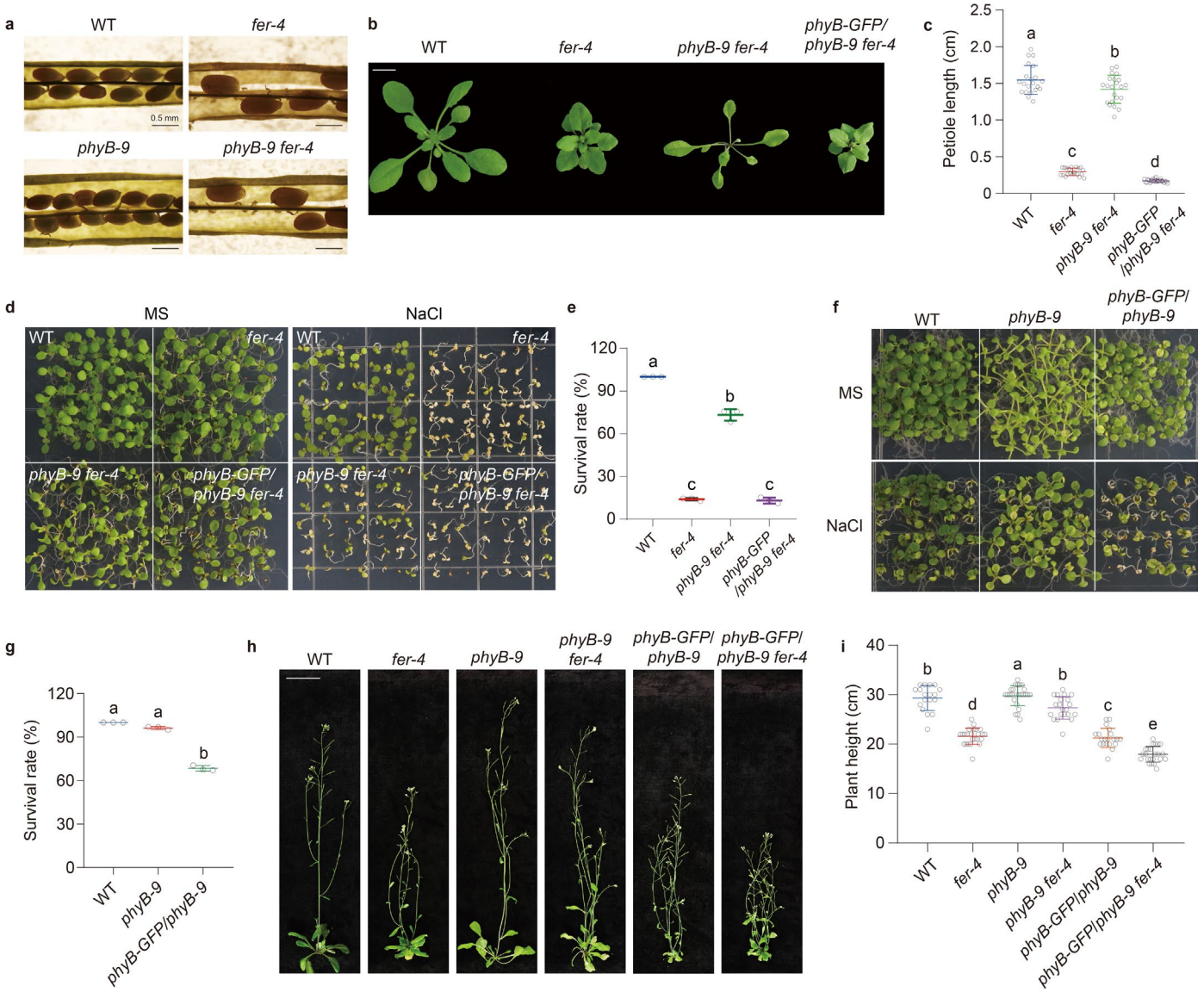

Extended Data Fig. 2 | *phyB* is involved in FER-mediated regulation of plant growth and salt tolerance. a, Representative images of wild type, *fer-4*, *phyB-9*, and *phyB-9 fer-4* siliques. Scale bar, 0.5 mm. **b**, Representative images of wild type, *fer-4*, *phyB-9 fer-4*, and *35 S::phyB-GFP/phyB-9 fer-4* grown on soils for 22 days under white light conditions (16 h light/8 h dark cycle). Scale bar, 1 cm. **c**, Quantification of the petiole length of plants shown in **b**. Values are the means ± SD (n = 21 plants). **d**, Phenotype of wild type, *fer-4*, *phyB-9 fer-4*, and *35 S::phyB-GFP/phyB-9 fer-4* grown on 1/2 MS media supplemented with or without NaCl (120 mM) under white light conditions. **e**, Quantification of the survival rate of seedlings grown on NaCl medium. Values are the means ± SD of three biological replicates. **f**, Phenotype of wild type, *phyB-9*, and *35 S::phyB-GFP/phyB-9* transgenic seedlings grown on 1/2 MS medium with or without NaCl (120 mM) under white light conditions. **g**, Quantification of the survival rate of seedlings grown on NaCl medium. Values are the means ± SD of three biological replicates. **h**, Representative images of wild type, *fer-4*, *phyB-9*, *phyB-9 fer-4*, *35 S::phyB-GFP/phyB-9*, and *35 S::phyB-GFP/phyB-9 fer-4* seedlings grown on soils for 35 days under white light conditions. Scale bar, 5 cm. **i**. Quantification of the plant height as shown in **h**. Values are the means ± SD (n = 18-25 plants). Different letters in **c**, **e**, **g** and **i** indicate statistically significant differences ($P < 0.01$, one-way ANOVA).

https://doi.org/10.1038/s41477-023-01390-4

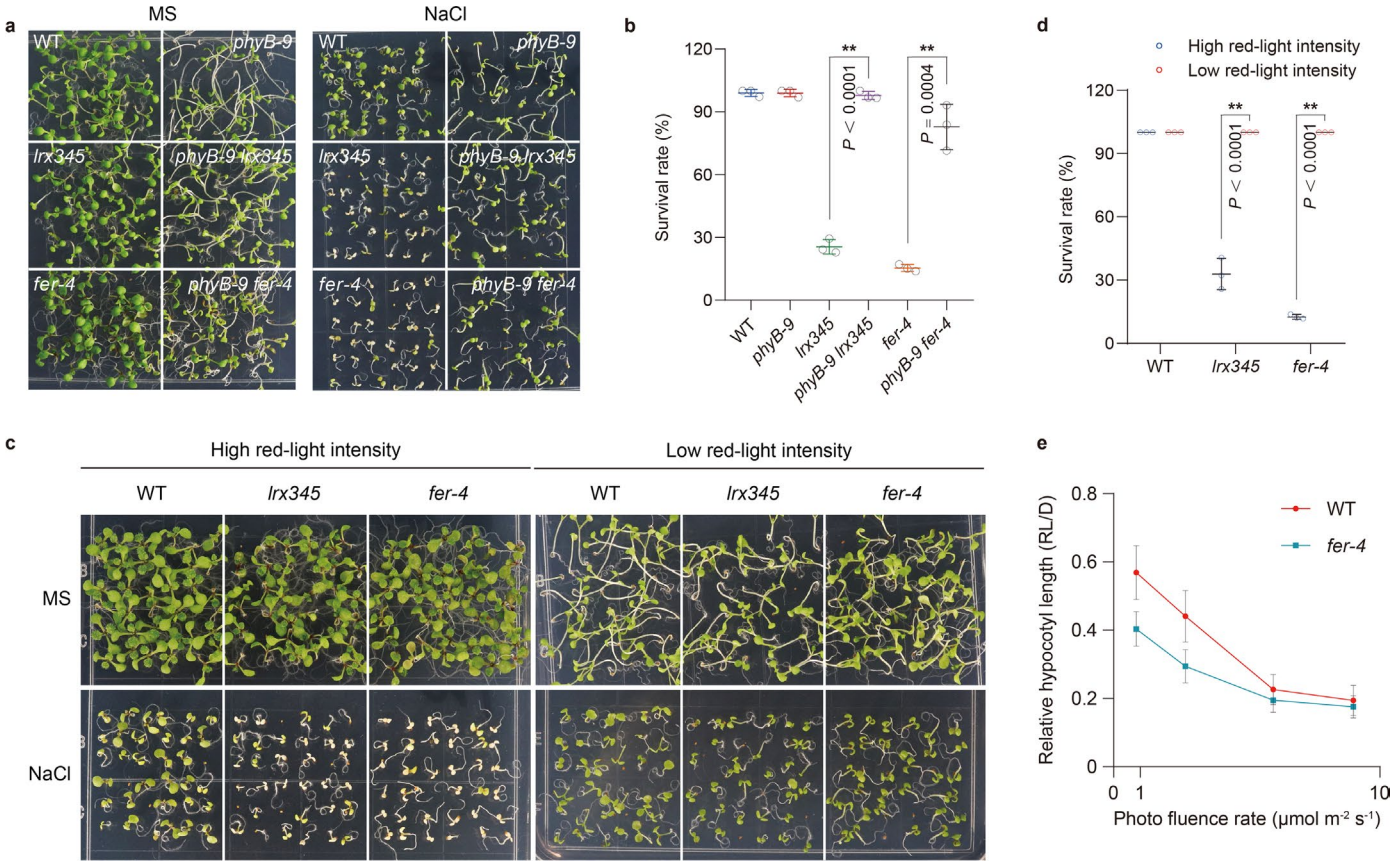

Extended Data Fig. 3 | *phyB* mutation suppresses the salt-hypersensitivity of the *lrx345* and *fer-4* mutants under monochromatic red light illumination. **a**, Phenotype of each genotype grown on 1/2 MS media supplemented with or without NaCl (120 mM) under continuous red light. **b**, Quantification of the survival rate of seedlings grown on NaCl medium as shown in **a**. Values are the means ± SD of three biological replicates. **c**, Phenotype of wild type, *lrx345*, and *fer-4* seedlings grown on 1/2 MS and 1/2 MS + NaCl (120 mM) media under continuous high red-light intensity (~15 μmol m-2 sec-1) or continuous low red-light intensity (~1 μmol m-2 sec-1). **d**, Quantification of the survival rate of seedlings grown on NaCl medium as shown in **c**. Values are the means ± SD of three biological replicates. **e**, Fluence rate response curves to analyze hypocotyl elongation inhibition under different red light fluence rates at 22 °C. Wild type and *fer-4* mutant were grown on 1/2 MS medium without sucrose in dark or continuous red light for 4 days. Relative hypocotyl length of the seedings grown under different red light fluence rates was calculated by comparing with that under dark conditions. Values are the means ± SD (n = 32-41 seedlings). Asterisks in **b** and **d** indicate statistically significant differences (**$P < 0.01$, Student's *t* test, two-sided).

https://doi.org/10.1038/s41477-023-01390-4

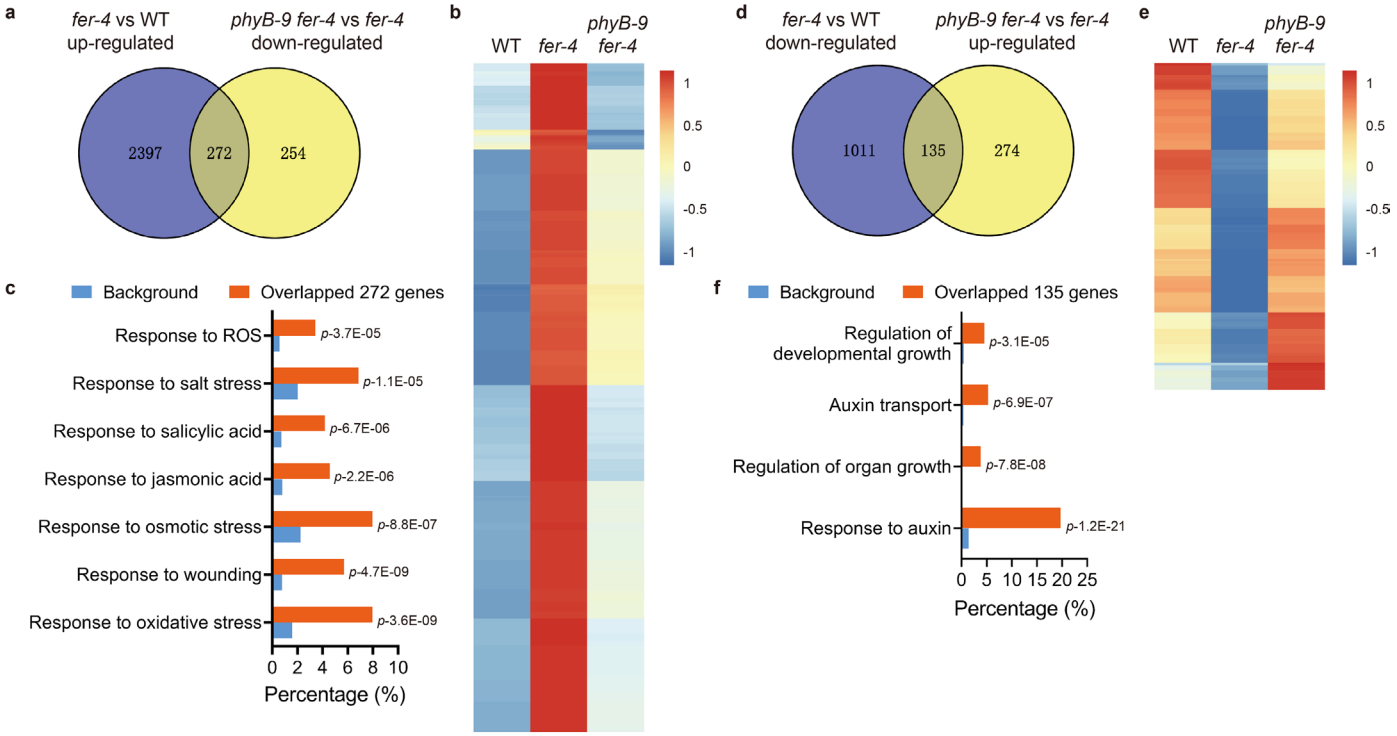

Extended Data Fig. 4 | Transcriptomic profiling reveals that FER regulates a subset of gene expression via phyB. a, Venn diagrams showing the overlapped genes that were up-regulated in *fer-4* mutant compared with wild type, but down-regulated in *phyB-9 fer-4* compared with *fer-4* mutant. **b**, Heat map of the 272 overlapped genes shown in **a**. **c**, GO enrichment analysis for the overlapped genes shown in **a**. Categories that were significantly enriched for these overlapped genes were selected and shown. Significance was determined using Student's *t* test (two-sided). **d**, Venn diagrams showing the overlapped genes that were down-regulated in *fer-4* mutant compared with wild type, but up-regulated in *phyB-9 fer-4* compared with *fer-4* mutant. **e**, Heat map of the 135 overlapped genes shown in **d**. **f**, GO enrichment analysis for the overlapped genes shown in **d**. Categories that were significantly enriched for these overlapped genes were selected and shown. Significance was determined using Student's *t* test (two-sided).

https://doi.org/10.1038/s41477-023-01390-4

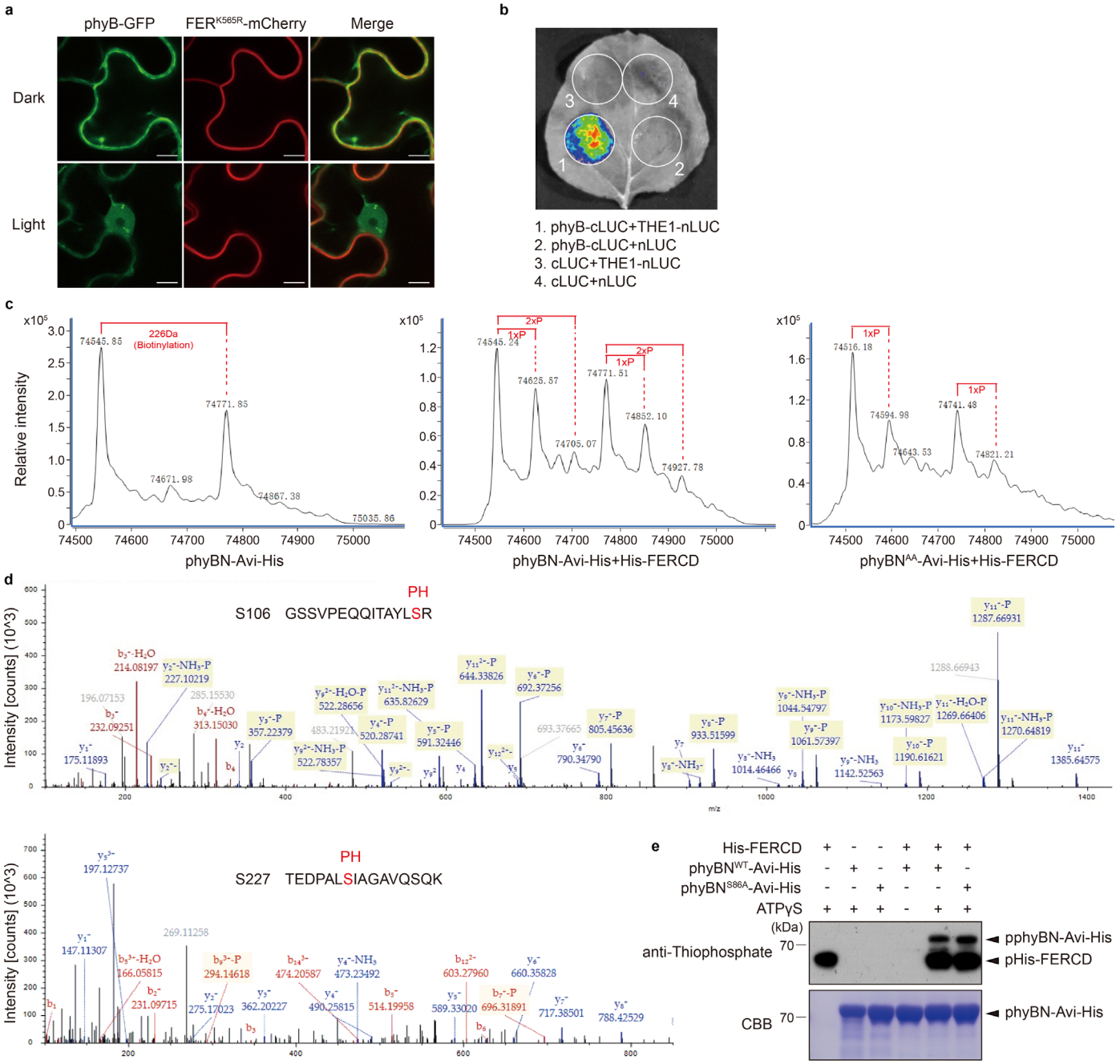

Extended Data Fig. 5 | Identification of the phosphorylation sites of phyB by FER. a, Co-localization analysis of FER and phyB in tobacco leaves under dark and white light conditions. Scale bar, 10 μm. **b**, Split luciferase complementation assay showing the interaction of THE1 with phyB. Fluorescence was detected at 48 h after infiltration of the indicated constructs. **c**, Mass spectrometry analysis of the phosphorylation of phyBN and phyBN^{AA} after incubation with FERCD. In the left panel, the two peaks represent nonphosphorylated phyBN and the biotin-tagged nonphosphorylated phyBN. In the middle and right panels, the newly developed peaks represent phosphorylated phyBN. **d**, The phosphorylation sites of phyB after incubation with FERCD were identified by LC–MS analysis. PH indicates the phosphorylated residues. **e**, In vitro kinase assay showing the phosphorylation of phyBN and phyBN^{S86A} by FERCD. It should be noted that, due to the addition of a small amount of FERCD in the reaction buffer, FERCD band was not clearly detected in CBB. The experiments in **a** and **e** were repeated independently for at least twice with similar results.

https://doi.org/10.1038/s41477-023-01390-4

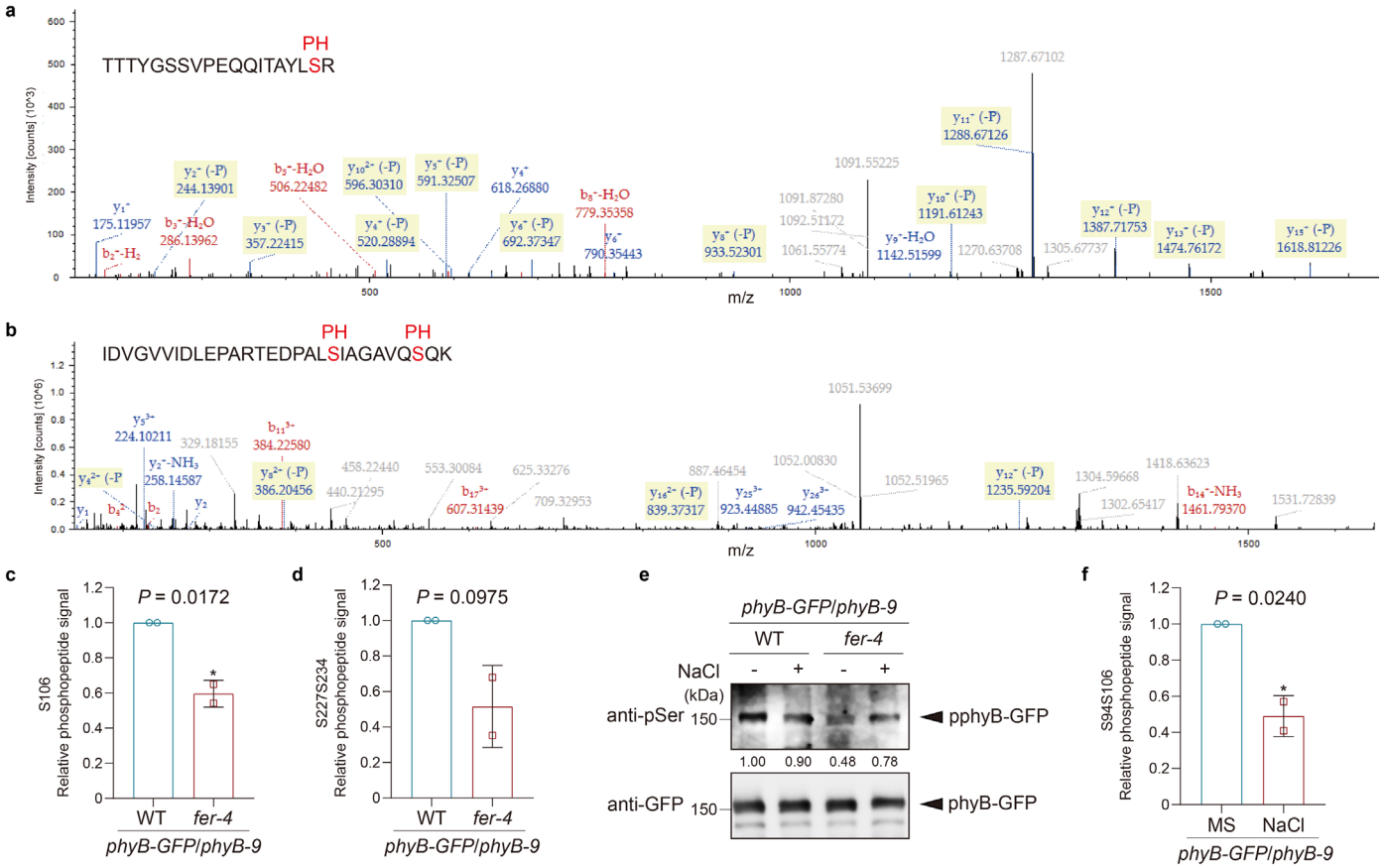

Extended Data Fig. 6 | Identification of the phosphorylation sites of phyB by FER in *Arabidopsis*. **a**,**b**, In vivo phosphorylations of S106 (**a**) and S227 (**b**) residues in phyB were identified by using LC–MS assay. PH indicates the phosphorylated residues. **c**,**d**, Relative phosphopeptide signals of the peptides containing phosphorylated S106 (**c**) or phosphorylated S227S234 (**d**) residues in wild type and *fer-4* seedlings based on LC–MS data. **e**, Analysis of the phosphorylation of phyB in wild type and *fer-4* seedlings grown on 1/2 MS medium with or without NaCl (120 mM). Total proteins were extracted from seven-day-old etiolated seedlings. phyB-GFP protein was immunoprecipitated with anti-GFP magarose beads, and immunoblotting assays were performed using anti-phosphoserine and anti-GFP antibodies. The experiment was repeated independently for twice with similar results. **f**, Relative phosphopeptide signals of the phyB peptides containing phosphorylated S94S106 residues in *Arabidopsis* seedlings treated with or without NaCl (150 mM). Values in **c**, **d** and **f** are the means ± SD of two biological replicates. Asterisks in **c** and **f** indicate statistically significant differences (*$P < 0.05$, Student's *t* test, two-sided).

https://doi.org/10.1038/s41477-023-01390-4

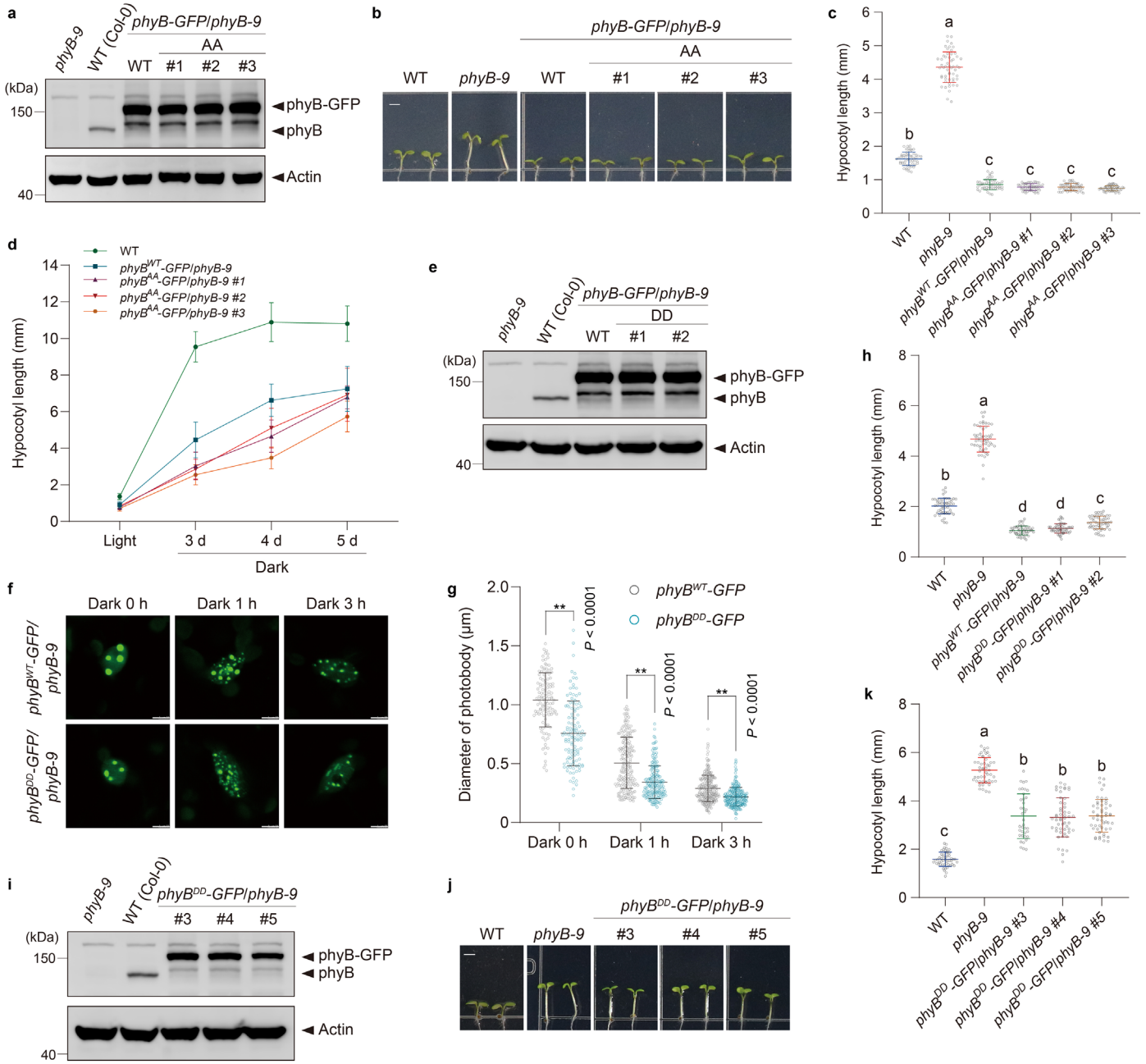

Extended Data Fig. 7 | Phosphorylation of Ser106 and Ser227 is required for the regulation of photobody dissociation under dark conditions. **a**, Protein abundance of phyB in wild type (Col-0), *35 S::phyB-GFP/phyB-9* (WT), and *35 S::phyB*^{S106AS227A}*-GFP/phyB-9* (AA) transgenic plants was analyzed using anti-phyB antibody. **b**, Hypocotyl phenotype of four-day-old seedlings grown on 1/2 MS medium under white light conditions (16 h light/8 h dark cycle). Scale bar, 2 mm. **c**, Quantification of the hypocotyl length of the seedlings shown in **b**. Values are the means ± SD (n = 50-55 seedlings). **d**, Time-course analysis of the hypocotyl length of seedlings before and after dark treatment (n = 33 seedlings). **e**, Protein abundance of phyB in each genotype was analyzed by using anti-phyB antibody. DD represents *35 S::phyB*^{S106DS227D}*-GFP/phyB-9* transgenic plants. **f**, Photobody dissociation under dark conditions. Five-day-old seedlings were exposed to white light for 5 h (ZT5) after dawn, and then the seedlings were treated in darkness for 1 h and 3 h before observation of photobodies. Scale bar, 4 μm. **g**, Quantification of the diameter of phyB photobodies shown in **f**. Values are the means ± SD (n > 100 bodies from 30-40 cells). **h**, Hypocotyl length of four-day-old seedlings grown on 1/2 MS medium under white light conditions. Values are the means ± SD (n = 54 seedlings). **i**, Protein abundance of phyB in each genotype was analyzed using anti-phyB antibody. **j**, Hypocotyl phenotype of four-day-old seedlings grown on 1/2 MS medium under white light conditions. Scale bar, 2 mm. **k**, Quantification of the hypocotyl length of the seedlings shown in **j**. Values are the means ± SD (n = 38-53 seedlings). Asterisks in **g** indicate statistically significant differences ($^{**}P < 0.01$, Student's *t* test, two-sided). Different letters in **c**, **h**, and **k** indicate statistically significant differences ($P < 0.01$, one-way ANOVA). The experiments in **a**, **e** and **i** were repeated independently for at least three times with similar results.

https://doi.org/10.1038/s41477-023-01390-4

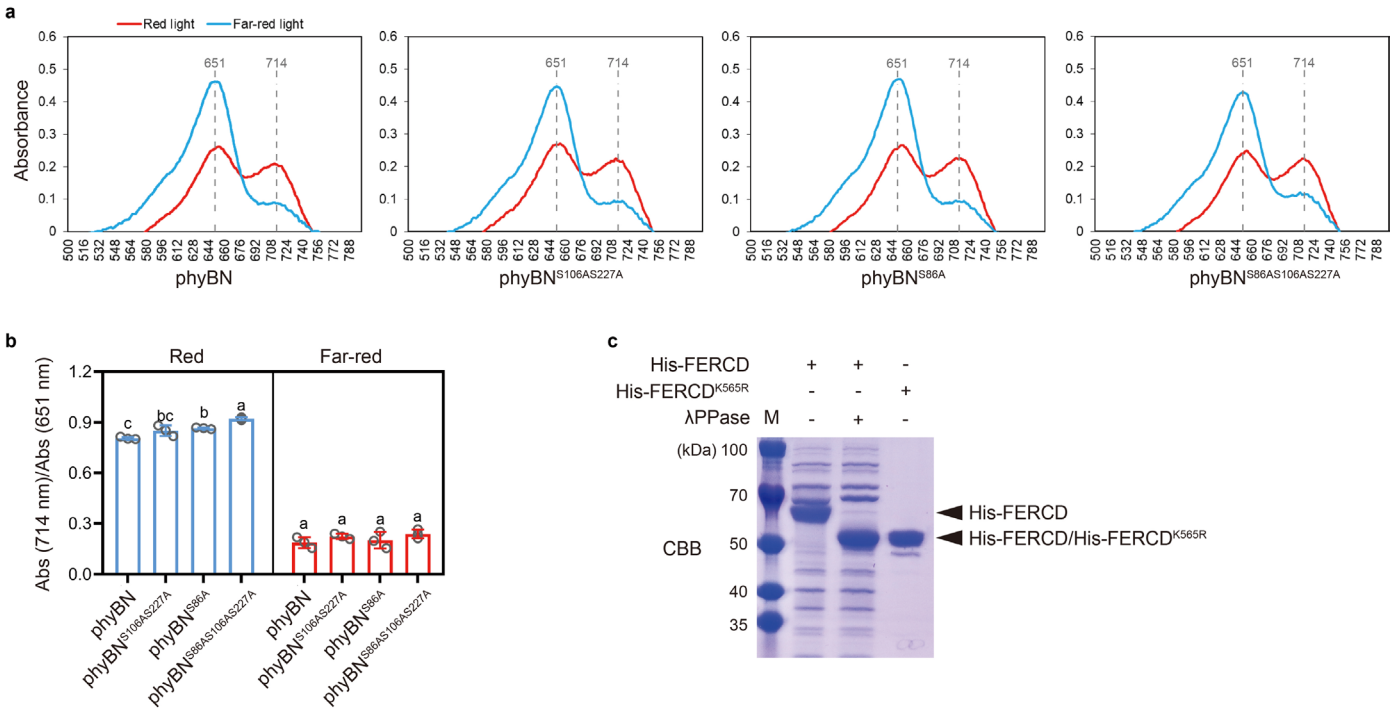

Extended Data Fig. 8 | Phosphorylation of phyB is not required for far-red light-triggered photoconversion. a, Spectral analysis of the photoswitching of wild type phyBN, phyBN^{S106AS227A}, phyBN^{S86A}, and phyBN^{S86AS106AS227A} after irradiance with far-red light. Proteins were exposed to red light illumination (~17 µmol m-2 sec-1) for 5 min and then exposed to far-red light illumination (~5 µmol m-2 sec-1) for 5 min. Red lines indicate absorbance spectra after red light illumination and blue lines indicate absorbance spectra after far-red light illumination. The absorption spectra of phyBN were measured using Nanodrop 2000C spectrophotometer. **b**, Quantification of the absorption spectra of the wild type phyBN and point-mutated phyB under red light and far-red light illumination. Y axis represents Pfr/Pr ratio. Values are the means ± SD of three independent replicates. Different letters indicate statistically significant differences ($p < 0.01$, one-way ANOVA). **c**, Recombinant His-FERCD and His-FERCD^{K565R} were detected by Coomassie Brilliant Blue (CBB) staining. His-FERCD was treated with or without λPPase. The experiments were repeated independently for three times with similar results.

https://doi.org/10.1038/s41477-023-01390-4

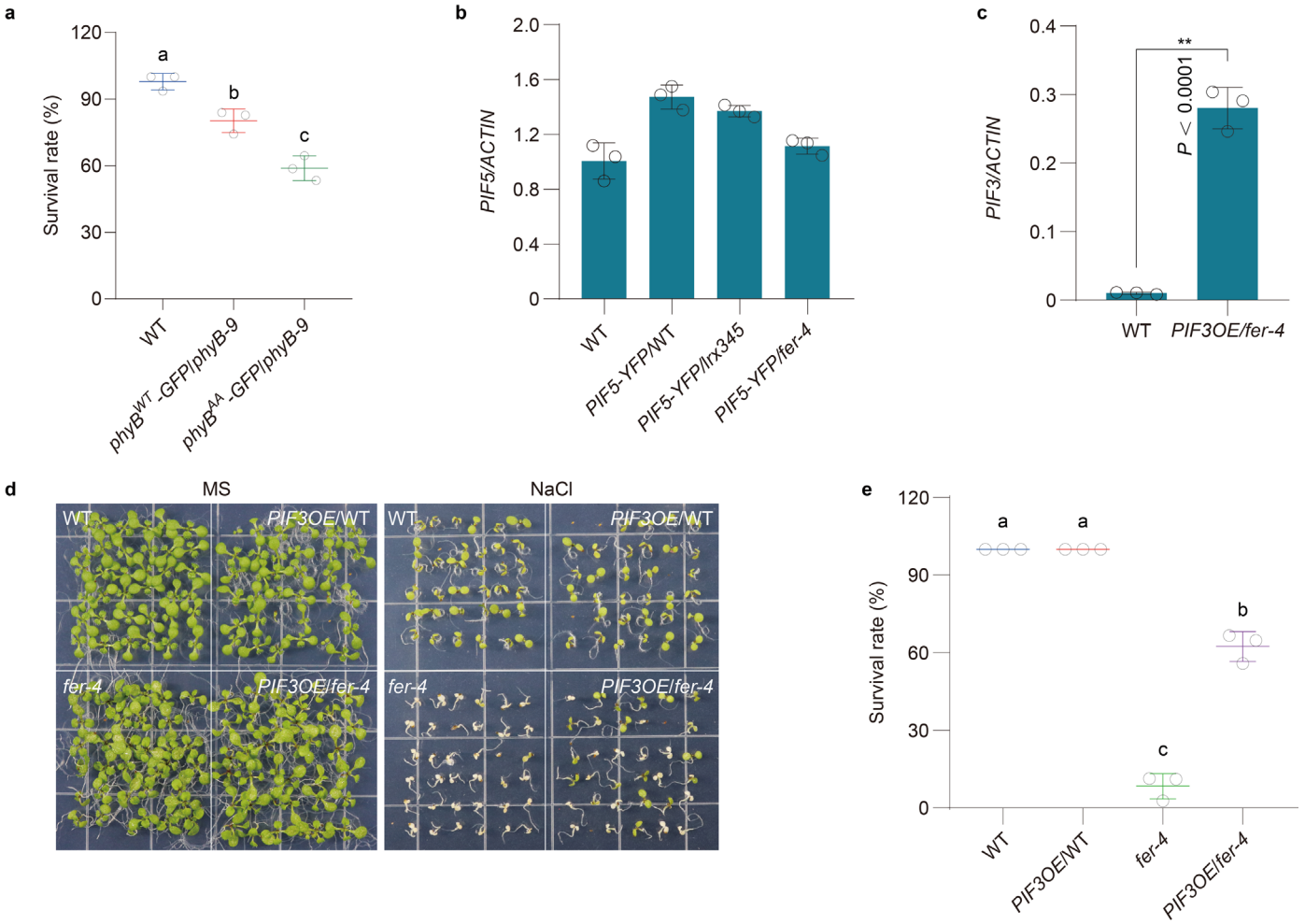

Extended Data Fig. 9 | phyB-PIFs module is required for the regulation of plant survival under salt stress. a, The survival rate of wild type, *35 S::phyB-GFP/phyB-9* and *35 S::phyB*^{S106AS227A}*-GFP/phyB-9* (AA) seedlings grown on 1/2 MS medium supplemented with NaCl (120 mM) under white light conditions (16 h light/8 h dark cycle). Values are the means ± SD of three independent replicates. **b**, RT–qPCR analysis of the transcript level of *PIF5* gene in wild type and *35 S::PIF5-YFP* transgenic plants. *ACTIN8* was used as an internal control. **c**, RT–qPCR analysis of the transcript level of *PIF3* gene in wild type and *PIF3OE/fer-4* seedlings. **d**, Phenotypes of wild type, *fer-4*, *PIF3OE*/WT, and *PIF3OE*/*fer-4* seedlings grown on 1/2 MS medium with or without NaCl (120 mM) under white light conditions. **e**, Quantification of the survival rate of seedlings grown on NaCl medium. Values in **a**, **b**, **c** and **e** are the means ± SD of three independent replicates. Different letters in **a** and **e** indicate statistically significant differences ($p < 0.01$, one-way ANOVA). Asterisks in **c** indicate statistically significant differences ($^{**}P < 0.01$, Student's *t* test, two-sided).

nature portfolio

Corresponding author(s): Chunzhao Zhao

Last updated by author(s): Feb 26, 2023

Reporting Summary

Nature Portfolio wishes to improve the reproducibility of the work that we publish. This form provides structure for consistency and transparency in reporting. For further information on Nature Portfolio policies, see our Editorial Policies and the Editorial Policy Checklist.

Statistics

For all statistical analyses, confirm that the following items are present in the figure legend, table legend, main text, or Methods section.

n/a	Confirmed	
☐	☒	The exact sample size (*n*) for each experimental group/condition, given as a discrete number and unit of measurement
☐	☒	A statement on whether measurements were taken from distinct samples or whether the same sample was measured repeatedly
☐	☒	The statistical test(s) used AND whether they are one- or two-sided *Only common tests should be described solely by name; describe more complex techniques in the Methods section.*
☒	☐	A description of all covariates tested
☒	☐	A description of any assumptions or corrections, such as tests of normality and adjustment for multiple comparisons
☐	☒	A full description of the statistical parameters including central tendency (e.g. means) or other basic estimates (e.g. regression coefficient) AND variation (e.g. standard deviation) or associated estimates of uncertainty (e.g. confidence intervals)
☐	☒	For null hypothesis testing, the test statistic (e.g. *F*, *t*, *r*) with confidence intervals, effect sizes, degrees of freedom and *P* value noted *Give P values as exact values whenever suitable.*
☒	☐	For Bayesian analysis, information on the choice of priors and Markov chain Monte Carlo settings
☒	☐	For hierarchical and complex designs, identification of the appropriate level for tests and full reporting of outcomes
☒	☐	Estimates of effect sizes (e.g. Cohen's *d*, Pearson's *r*), indicating how they were calculated

Our web collection on statistics for biologists contains articles on many of the points above.

Software and code

Policy information about availability of computer code

Data collection	NightShade LB985 was used to detect fluorescence in split luciferase complementation assay. Confocal microscopy was performed with a Leica TCS SMD FLCS confocal laser scanning microscope. Nanodrop 2000C was used for spectral analysis of recombinant phyB protein. Easy nLC 1200 chromatographic system was used for chromatographic separation. QE HFX was used to obtain the LC-MS data.
Data analysis	ImageJ 1.53c was used for microscopic image and immunoblotting analysis. GraphPad Prism 8.0.1, Microsoft Office Excel, and IBM SPSS statistics 20 were used for statistical analysis. HISAT2 version 2.2.1 and R package edgeR 3.24.3 were used for RNA-Seq data analysis. Venn diagrams were performed by Venny 2.1 (https://bioinfogp.cnb.csic.es/tools/venny/index.html). GO enrichment analysis was performed by AgriGO v2.0 (http://systemsbiology.cau.edu.cn/agriGOv2/index.php). Proteome Discoverer 2.4 was used for LC-MS data analysis.

For manuscripts utilizing custom algorithms or software that are central to the research but not yet described in published literature, software must be made available to editors and reviewers. We strongly encourage code deposition in a community repository (e.g. GitHub). See the Nature Portfolio guidelines for submitting code & software for further information.

Data

Policy information about availability of data

All manuscripts must include a data availability statement. This statement should provide the following information, where applicable:

- Accession codes, unique identifiers, or web links for publicly available datasets
- A description of any restrictions on data availability
- For clinical datasets or third party data, please ensure that the statement adheres to our policy

All materials in this study are available from the corresponding author upon request. The raw data of BSA sequencing used in this study have been deposited in the NCBI BioProject database under accession number PRJNA914087. RNA-seq data used in this study have been deposited in the NCBI GEO under accession number GSE188335. Arabidopsis reference genome (TAIR10) was used in this study. Source data are provided with this paper.

Human research participants

Policy information about studies involving human research participants and Sex and Gender in Research.

Reporting on sex and gender	N/A
Population characteristics	N/A
Recruitment	N/A
Ethics oversight	N/A

Note that full information on the approval of the study protocol must also be provided in the manuscript.

Field-specific reporting

Please select the one below that is the best fit for your research. If you are not sure, read the appropriate sections before making your selection.

☒ Life sciences ☐ Behavioural & social sciences ☐ Ecological, evolutionary & environmental sciences

For a reference copy of the document with all sections, see nature.com/documents/nr-reporting-summary-flat.pdf

Life sciences study design

All studies must disclose on these points even when the disclosure is negative.

Sample size	Sample size was chosen based on similar studies in this filed to allow for confident statistical analysis (Zhao et al., 2018, PNAS; Zhao et al., 2021, National Science Review). For survival rate analysis under salt stress in Arabidopsis, a minimum of 25 plants were used for each genotype. For other phenotypic analysis, the sample size is indicated in figure legends.
Data exclusions	No data were excluded from analysis.
Replication	All experimental data were repeated in several independent biological replicates (n). The number of repeats is indicated in figure legends. All phenotypic analysis in this study were repeated at least three times. All Y2H and split-LUC assays were repeated at least three times. For other immunoblot assays, a minimum of two independent biological replicates were performed.
Randomization	Plant pots and plates positioning in the growth chambers were randomized to minimize positional effects during growth. Plants of each genotype were randomly collected for analysis.
Blinding	No blinding was applied in this study because the different genotypes show obvious developmental phenotypes, so it is hard for investigators to be blinded to perform experiments and collect data.

Reporting for specific materials, systems and methods

We require information from authors about some types of materials, experimental systems and methods used in many studies. Here, indicate whether each material, system or method listed is relevant to your study. If you are not sure if a list item applies to your research, read the appropriate section before selecting a response.

Materials & experimental systems

n/a	Involved in the study
☐	☒ Antibodies
☒	☐ Eukaryotic cell lines
☒	☐ Palaeontology and archaeology
☒	☐ Animals and other organisms
☒	☐ Clinical data
☒	☐ Dual use research of concern

Methods

n/a	Involved in the study
☒	☐ ChIP-seq
☒	☐ Flow cytometry
☒	☐ MRI-based neuroimaging

Antibodies

Antibodies used

1. Mouse monoclonal anti-GFP, Sigma, Cat#11814460001, RRID:AB_390913, 1:3000 dilution, clones 7.1 and 13.1
2. Mouse monoclonal anti-phyB, PhytoAB, Cat#PHY1733, 1:2000 dilution, clone 10P5
3. Rabbit monoclonal anti-Thiophosphate ester, Abcam, Cat#ab92570, :AB_10562142, 1:5000 dilution, clone 51-8
4. Mouse monoclonal anti-Actin, Agrisera, Cat#AS164111, 1:5000 dilution, clone 14H4G8
5. Rabbit polyclonal anti-PEPC, Agrisera, Cat#AS09458, RRID:AB_2063166, 1:2000 dilution, clone C91-301
6. Rabbit polyclonal anti-Histone H3, Millipore, Cat#07-690, RRID:AB_417398, 1:10000 dilution
7. Rabbit monoclonal anti-Myc, Cell Signaling Technology, Cat#2278, RRID:AB_490778, 1:1000 dilution, clone 71D10
8. Rabbit polyclonal anti-PIF5, Agrisera, Cat#AS122112, 1:1000 dilution
9. Rabbit polyclonal anti-Phosphoserine, Abcam, Cat#ab9332, 1:125 dilution
10. Goat anti-mouse IgG (H+L) HRP conjugate, Bio-rad, Cat# 1721011, RRID:AB_2617113, 1:10000 dilution
11. Goat anti-rabbit IgG (H+L) HRP conjugate, Bio-rad, Cat# 1721019, RRID:AB_11125143, 1:10000 dilution

Validation

1. https://www.sigmaaldrich.cn/CN/en/product/roche/11814460001
2. https://www.phytoab.com/phyb-anti-phytochrome-b-antibody-2085?___SID=U
3. https://www.abcam.cn/thiophosphate-ester-antibody-51-8-ab92570.html
4. https://www.agrisera.com/cgi-bin/ibutik/AIR_ibutik.fcgi
5. https://www.agrisera.com/en/artiklar/pepc-phosphoenolpyruvate-carboxylase.html
6. https://www.sigmaaldrich.cn/CN/en/product/mm/07690
7. https://www.cellsignal.com/products/primary-antibodies/myc-tag-71d10-rabbit-mab/2278
8. https://www.agrisera.com/en/artiklar/pif5-phytochrome-interacting-factor-5.html
9. https://www.abcam.cn/phosphoserine-antibody-ab9332.html
10. https://www.bio-rad.com/en-cn/sku/1721011-goat-anti-mouse-igg-hl-hrp-conjugate?ID=1721011
11. https://www.bio-rad.com/en-cn/sku/1721019-goat-anti-rabbit-igg-hl-hrp-conjugate?ID=1721019